Mon. Not. R. Astron. Soc. **000**, 1–27 (2013) Printed 23 March 2016 (MN LATEX style file v2.2)

MAGGIE: Models and Algorithms for Galaxy Groups, Interlopers and Environment

Manuel Duarte⋆ and Gary A. Mamon†
Institut d'Astrophysique de Paris (UMR 7095: CNRS & UPMC, Sorbonne Universités), F–75014 Paris, France

arXiv:1412.3364v3 [astro-ph.CO] 22 Mar 2016

Accepted 2015 August 3. Received 2015 August 3; in original form 2014 December 10; Consolidated version with Erratum

ABSTRACT

Combining our knowledge of halo structure and internal kinematics from cosmological dark matter simulations and the distribution of halo interlopers in projected phase space measured in cosmological galaxy simulations, we develop MAGGIE, a prior- and halo-based, probabilistic, abundance matching (AM) grouping algorithm for doubly complete subsamples (in distance and luminosity) of flux-limited samples. We test MAGGIE-L and MAGGIE-M (in which group masses are derived from AM applied to the group luminosities and stellar masses, respectively) on groups of at least three galaxies extracted from a mock Sloan Digital Sky Survey Legacy redshift survey, incorporating realistic observational errors on galaxy luminosities and stellar masses. In comparison with the optimal Friends-of-Friends (FoF) group finder, groups extracted with MAGGIE are much less likely to be secondary fragments of true groups; in primary fragments, its galaxy memberships (relative to the virial sphere of the real-space group) are much more complete and usually more reliable, and its masses are much less biased and usually with less scatter, as are its group luminosities and stellar masses (computed in MAGGIE using the membership probabilities as weights). FoF outperforms MAGGIE only for high-mass clusters: for the reliability of the galaxy population and the dispersion of its total mass. In comparison with our implementation of the Yang et al. group finder, MAGGIE reaches much higher completeness and slightly lower group fragmentation and dispersion on group total masses, luminosities and stellar masses, but slightly greater bias in the latter two and lower reliabilities. MAGGIE should therefore lead to sharper trends of environmental effects on galaxies and more accurate mass/orbit modelling.

Key words: methods: numerical – galaxies: clusters: general – galaxies: groups: general – dark matter.

1 INTRODUCTION

In the hierarchical growth of structure in the Universe, dominated by gravity (and dark energy), matter flows from low to high density regions. To first order, galaxies, which form in small dark matter haloes, follow this evolution and cluster into galaxy systems called *clusters* or *groups*, depending on their mass (clusters are often defined with masses within the virial radius greater than $10^{14}\mathrm{M}_{\odot}$).

The properties of galaxies within these systems (hereafter denoted *groups* for simplicity), now attached to dark matter *subhaloes*, are likely to be modified by the peculiar environment of their parent groups. Many physical processes should indeed alter galaxy properties in groups: the high galaxy density in groups will lead to galaxy interactions and possibly mergers; the deeper gravitational potentials of the more massive groups will produce higher velocity dispersions for the galaxy population, favouring rapid flybys over mergers (e.g., Mamon 1992); the tides from the group potential will prevent outer gas from accreting onto galaxy disks (Larson et al. 1980); the diffuse intra-group gas will exert ram pressure on the galaxy's gas (Gunn & Gott 1972) and either compress it, enhancing star formation (e.g., Kennicutt et al. 1984), or when the pressure gets very high it will expel the gas (Gunn & Gott), decreasing subsequent star formation.

Galaxy groups and clusters thus represent an ideal laboratory to test the environmental effects on galaxies in models of galaxy formation and evolution. Groups and clusters are also an important tool to probe cosmological parameters, such as the dark energy parameter (Wang & Steinhardt 1998). Moreover, clusters have been recently used to test a major prediction of general relativity, with the recent discovery of weak but significant signs of gravitational redshifts (Wojtak et al. 2011).

Since the early discovery of morphological segregation of galaxies in clusters (Shapley 1926; Hubble 1936; van den Bergh 1960), i.e. where inner regions of clusters preferentially contain elliptical galaxies, whose red colours are indicative of old stellar populations, it has been clear that the efficiency with which stars form within galaxies must depend on their environment. In other

⋆ E-mail: acanthostega@hotmail.fr
† E-mail: gam@iap.fr

© 2013 RAS

words, high density environments act to *quench* star formation in galaxies. More specifically, the specific star formation rate (SSFR) of galaxies (star formation rate divided by stellar mass) is likely to be a function of two separate environmental parameters: the *global environment* characterized by the total mass of their group, and the *local environment* that measures the position of the galaxy within its group.

Peng et al. (2010) studied the dependence of SSFR with stellar mass and environment, where they quantified the latter by the distance to the 5th nearest neighbour. They found that, at low stellar mass, the SSFR varied more with the density of the environment, while at high mass, the environmental effects are small and the SSFR anti-correlates with stellar mass. Unfortunately, the use of an environment tracer such as the 5th nearest neighbour produces a mix between the global and local environments. In contrast to Peng et al., Weinmann et al. (2006) and von der Linden et al. (2010) both considered indicators of both the global and local environments. Weinmann et al. found that the fraction of late-type satellite galaxies appears more anti-correlated with group mass than with stellar mass, while von der Linden et al. found that high-mass galaxies also show some moderate dependence of SSFR with the relative distance to the group/cluster centre (albeit limited to low cluster-centric radii).

These possible disagreements highlight the importance of properly measuring the global and local environments. Unfortunately, a clean characterization of the *real space* environment from the *redshift space* observed distribution of galaxies is difficult since the *redshift distortions* (Jackson 1972) caused by the velocity dispersion of the galaxy group distorts the group into elongated structures pointing towards the observer, i.e. Fingers-of-God (Tully & Fisher 1978). Moreover, because of redshift distortions, real space groups can be merged into single groups in redshift space. Conversely, grouping algorithms inevitably lead to some fragmentation of real-space groups, so that the secondary fragments do not represent bona-fide groups of their own (although some may represent subgroups of real-space groups). Finally, even without group merging and fragmentation, a group finder may miss some of the real-space group galaxies, leading to incomplete galaxy membership; or conversely may include additionally galaxies that lie outside of the virial sphere of the real space group, producing unreliable galaxy membership. One then wonders to what extent the strength of environmental effects on galaxy properties may be washed out by the imperfect extraction of the global and local environments by the grouping algorithm (group finder).

Many galaxy group catalogues have already been published, usually following the first publications of data from galaxy surveys. First attempts were made with visual selections based on well-defined criteria (Abell 1958; Zwicky et al. 1961 for clusters and Rose 1977; Hickson 1982 for compact groups). The first automated (and simple) algorithm has been the percolation '*Friends-of-Friends*' (FoF) method, first introduced by Turner & Gott (1976) and Huchra & Geller (1982), in which groups are built by collections of galaxies linked, two-by-two, by their proximity. Redshift distortions are taken into account by the use of two different linking lengths, along the line-of-sight (LOS) and transverse directions. There is a fairly wide range of pairs of linking lengths used in the literature. In a previous study (Duarte & Mamon 2014, hereafter Paper I), we have analysed several mock SDSS samples of galaxies to optimize the pairs of linking lengths for minimal group fragmentation and merging, maximal galaxy completeness and reliability, and maximal group mass accuracy (see also Eke et al. 2004, Berlind et al. 2006, and Robotham et al. 2011), and compared their optimal linking lengths with those of ten previous implementations of the FoF algorithm. Another fairly non-parametric grouping algorithm is to partition redshift space into Voronoi cells, constructed from Delaunay triangulation, providing local galaxy number densities that are inversely proportional to the volumes of the Voronoi cells (Marinoni et al. 2002, see also Gerke et al. 2005).

Building on our recently gained knowledge from cosmological N-body simulations, grouping algorithms have begun to appear, where priors on galaxy group properties are incorporated to improve their extraction from galaxy redshift surveys. In pioneering studies, Yang et al. (2005, 2007) developed an iterative method halo-based group finder that uses a density contrast criterion in *projected phase space* (PPS, i.e. projected radius and LOS velocity dispersion), assuming a Navarro, Frenk, & White (1996, hereafter NFW) surface density profile and a Maxwellian LOS velocity distribution, both in reasonably good agreement with what is found in the group- and cluster-mass haloes of dissipationless cosmological simulations. In the Yang et al. (2005, 2007) group finder, the group masses, hence virial radii, are determined by *abundance matching* (AM, first introduced by Marinoni & Hudson 2002), which assumes a one-to-one correspondence between group luminosity or stellar mass and its total (halo) mass to match the cumulative distribution functions (CDFs) of the cosmic halo mass function (HMF) and the group luminosity or stellar mass function (measured, here, in the previous iteration of the algorithm). AM between groups and haloes has also been introduced by Muñoz-Cuartas & Müller (2012) in their FoF algorithm that links haloes rather than galaxies: they consider halo virial radii in the transverse direction and maximum circular velocity in the LOS direction, combining the two links in an ellipsoidal fashion.

But galaxy surveys come with observational problems that are difficult to handle: surveys suffer from edge effects and from bright (saturated) stars masking regions, and those with photometric redshifts have large and sometimes catastrophic redshift errors. Probabilistic methods appear to be a promising way to deal with these aspects. For example, Liu et al. (2008) designed a probabilistic FoF method for surveys with photometric redshifts, Ascaso et al. (2012) incorporated priors on the galaxy luminosity function, while Rykoff et al. (2014) assumed a prior on the existence of the Red Sequence (see also Gladders & Yee 2000). Domínguez Romero et al. (2012) have recently adapted the Yang et al. group finder into a probabilistic algorithm: they initially assign haloes to single galaxies, and use AM like Yang et al. to assign group masses and radii. But Domínguez Romero et al. end their algorithm with a hard assignment of galaxies to their groups.

These studies can be improved in several respects:

(i) In their prediction of the density in PPS, Yang et al. (2005, 2007) and Domínguez Romero et al. (2012) assume that the LOS velocity dispersion is independent of projected radius, while cosmological N-body simulations (starting with Cole & Lacey 1996) indicate a convex profile in log-log. One can easily predict this LOS velocity dispersion profile (see Mamon & Łokas 2005 for a single integral expression) by solving the Jeans equation of local dynamical equilibrium, adopting the velocity anisotropy profile of the particles in the haloes of ΛCDM cosmological simulations (hereafter ΛCDM haloes).

(ii) Yang et al. (2005, 2007) and Domínguez Romero et al. (2012) assume that the LOS velocity distribution is Maxwellian, whereas the velocity anisotropy alters this Gaussianity (Merritt 1987), hence one can do better and predict its precise shape from the three-dimensional velocity distribution (Mamon, Biviano, & Boué 2013).

(iii) Rather than use a threshold in the PPS density as proposed

by Yang et al. (2005, 2007) and Domínguez Romero et al. (2012), one can take advantage of our knowledge of the distribution of galaxies in PPS for two terms: a) the galaxies within the virial sphere of the parent real-space group (hereafter the *halo* term); b) the galaxies that are in the virial cone but outside the virial sphere (hereafter the *interloper* term). The interloper PPS density was quantified by Mamon, Biviano, & Murante (2010) using a cosmological simulation, and it turns out to be fairly independent of halo mass (for cluster-mass haloes). Comparing the PPS densities from the halo and interloper terms yields a probability of membership. There is no need to perform a hard assignment of galaxies to groups in the end as was done by Domínguez Romero et al. (2012): group properties are easily obtained using the membership probabilities as weights.

(iv) Yang et al. (2007) employ a complicated and imprecise scheme (see their fig. 4) to estimate how the luminosity incompleteness varies with redshift in their flux-limited sample. Errors in the luminosity incompleteness will propagate, among other places, to the AM technique they use to infer group masses. However, the issue can be entirely avoided by restricting the group finder to subsamples that are doubly complete in both distance and luminosity. Admittedly, such samples are, at best, less than one-third the size of the parent flux-limited samples (see Tempel et al. 2014 for the SDSS). However, the very large sizes of the samples from recent or ongoing galaxy spectroscopic surveys (250 000 for the Two Degree Field Galaxy Redshift Survey [2dFGRS, Colless et al. 2001], 125 000 for the Six Degree Field Galaxy Survey [6dFGS, Jones et al. 2009], 700 000 for the primary spectroscopic sample of the Sloan Digital Sky Survey [SDSS, Abazajian et al. 2009], 300 000 for the ongoing Galaxy and Mass Assembly survey [GAMA, Hopkins et al. 2013]) lead to substantial sizes for doubly complete subsamples, which can be used for studies of environmental effects on galaxies. Moreover, it is wiser to study environmental effects on a group catalogue derived from a doubly-complete galaxy subsample, rather than start with a group catalogue derived from a flux-limited subsample and then cut it into a doubly complete subsample of groups to study environmental effects. For example, Tempel et al. (2014) have recently produced publicly available FoF group catalogues that they had run on doubly-complete SDSS galaxy subsamples.

(v) Yang et al. (2005, 2007), Muñoz-Cuartas & Müller (2012) and Domínguez Romero et al. (2012) wisely test their grouping algorithms using mocks. However, their adopted definitions for purity and contamination take values above (and below) unity, while we prefer a measure of the reliability that is restricted to values between zero and unity (see Sect. 3.3 below). Moreover, these mocks should include observational errors (on galaxy luminosities and stellar masses), and while this is briefly mentioned by Yang et al. (2005), it is not clear what level of errors were considered by them and Yang et al. (2007), while observational errors were not mentioned by Domínguez Romero et al..

In this work, we present a new probabilistic grouping algorithm, Models and Algorithms for Galaxy Groups, Interlopers and Environment, a.k.a. MAGGIE. The galaxy membership of MAGGIE groups is determined probabilistically, combining the distribution of interlopers in PPS measured by Mamon et al. (2010) with a realistic model for the distribution in PPS of halo members, while the group masses are determined by AM in an iterative fashion, as in Yang et al. (2005, 2007).

We present MAGGIE in Sect. 2, and our mocks and testing procedure are described in Sect. 3. We compare, in Sect. 4, the optimal FoF group finder with two implementations of MAGGIE, on their ability to recover physical properties and galaxy membership of real-space groups, we discuss our findings in Sect. 5 and summarize our results in Sect. 6.

2 MAGGIE

We present here a complete description of the different steps of MAGGIE. We start with a basic description of the algorithm, and then we explain how we take into account the edges of the galaxy sample.

2.1 Basic Group Finder

We assume that we have a galaxy sample that is doubly complete in distance and luminosity, with positions on the sky (right ascension and declination), redshifts, as well as apparent magnitudes in a given waveband and/or stellar masses. This is the minimum required data set.

MAGGIE groups are built around the most luminous galaxy (MAGGIE-L) or the most massive in stars (MAGGIE-M). This galaxy is assumed to be the *central galaxy* and at rest relative to the group. Although the most massive group galaxies can be offset and not at rest with the group (e.g., Skibba et al. 2011), we prefer this definition to the barycentre, since the galaxy number density profiles in clusters are known to be less cuspy when clusters are centered on their barycentres (Beers & Tonry 1986), and indeed most analyses adopt the central galaxy as the position of the group centre.

MAGGIE then builds groups with the following iterative method. Steps 2 to 4 are similar to those of Yang et al. (2005, 2007).

(1) *Sort galaxies by decreasing stellar mass and loop over potential groups*
We loop over the potential group central galaxies, sorted by decreasing galaxy stellar mass (MAGGIE-M) or luminosity (MAGGIE-L), performing the following steps:

(2) *Group total masses*

(2a) *Initial group total masses* On first pass, we determine the mass of each group, either by adopting group masses $M = 300\,L_r$ (MAGGIE-L) or using the relation between halo mass and central galaxy stellar mass (MAGGIE-M) that Behroozi, Conroy, & Wechsler (2010) derived from AM (basically matching the halo mass and central galaxy stellar mass CDFs). This initial choice has no effect on the final outcome (see Sect. 5.3.1).

(2b) *Group total masses on subsequent iterations* On subsequent passes, we determine the group mass by performing our own AM between our group luminosity (MAGGIE-L) or group stellar mass (MAGGIE-M) function (determined in the previous pass) and a chosen HMF:

$$N(>L_{\rm group}) = N(>M) \qquad (\text{MAGGIE-L}) \tag{1}$$

$$N(>m_{\rm group}) = N(>M) \qquad (\text{MAGGIE-M})\,, \tag{2}$$

where M is the group (halo) total mass, while $L_{\rm group}$ and $m_{\rm group}$ and represent the group luminosity and stellar mass, respectively.[1] (In this AM, we must assume that the group has the same central galaxy as in the previous iteration, which is true for

[1] We denote stellar masses as m and total (group/halo) masses (including dark matter and gas) as M.

the great majority of groups.) The cumulative mass functions are considered for the comoving volume of the subsample, i.e.

$$N(>M) = \int_{z_{\rm min}}^{z_{\rm max}} \left(\frac{{\rm d}V}{{\rm d}z}\right) {\rm d}z \int_M^\infty f(M',z)\,{\rm d}M' \,, \tag{3}$$

where $f(M)$ is the differential HMF. Numerically solving equation (1) or (2) together with equation (3) provides the group total mass as a function of the group luminosity or stellar mass. Practical details on the HMF are provided in Sect. 5.3.2.[2]

(3) *Group radii*
We estimate the group radius from the group mass, using

$$r_{200} = \left[\frac{G\,M_{200}}{100\,H^2(z)}\right]^{1/3} \,, \tag{4}$$

where r_{200} is our proxy for the virial radius and is the radius of the sphere (hereafter, *virial sphere*) centered on the position of the central galaxy and whose mean density is 200 times the *critical density* of the Universe, $\rho_{\rm crit} = 3H^2(z)/(8\,\pi G)$, while M_{200} is the mass within the virial sphere. The Hubble constant, in equation (4), for a flat Universe, is

$$H(z) = H_0\,\sqrt{\Omega_{\rm m}(1+z)^3 + 1 - \Omega_{\rm m}} \,, \tag{5}$$

where $\Omega_{\rm m}$ is the cosmological density parameter at $z = 0$. The factor 100 in equation (4) is really $\Delta/2$ for the overdensity relative to critical of $\Delta = 200$.[3]

(4) *Coordinates in projected phase space*
The projected separation R (hereafter, *projected radius*) and LOS velocity v of a galaxy relative to a central group galaxy (assumed at rest in the group) are written with the standard cosmological formulae:

$$R = \theta\, d_{\rm ang}(z_{\rm group}) \,, \tag{6}$$

$$v = c\,\frac{(z - z_{\rm group})}{1 + z_{\rm group}} \,, \tag{7}$$

where θ is the angular separation, c is the speed of light,

$$d_{\rm ang}(z) = \frac{c}{1+z}\int \frac{{\rm d}z'}{H(z')}$$

is the cosmological angular distance (for a flat Universe), and $z_{\rm group}$ is the redshift of the central group galaxy.[4]

[2] In this work, the cumulative HMF $N(>M)$ is derived by a maximum likelihood estimate of the parameters of the analytical differential HMF of Tinker et al. (2008) to the list of halo masses (within the sphere of radius r_{200}) of the the Millennium-II simulation from which our mocks were built. A theoretical HMF can be chosen when working on real data. Also, while it would be preferable to fit an analytical form to the group luminosity function or stellar mass function, to avoid shot noise and cosmic variance, such a fit is difficult with a single or double Schechter 1976 function. We therefore use the raw list of luminosities or stellar masses for the AM. We solve equation (1) or equation (2) by performing linear interpolation (in log-log space) of the cumulative HMF (which is not analytical despite the analytical nature of the differential HMF).

[3] Note that Yang et al. (2007) use virial radii corresponding to mean densities equal to 180 times the *mean density* of the Universe, which for their assumed $\Omega_{\rm m} = 0.238$ corresponds to 43 times the critical density of the Universe. For typical NFW density profiles, the virial radius used by Yang et al. is roughly $1.86\,(c/10)^{-0.052}$ times the radius r_{200} used here.

[4] In this article, all instances of the symbol v represent line-of-sight velocities of galaxies relative to the group.

(5) *Membership probability*
In MAGGIE, galaxies are not assigned to groups, but are provided with probabilities that they belong to a given group, i.e. to the virial sphere of the real-space group.
The probability that a galaxy lies within the virial sphere of the real space group is necessarily zero if the galaxy is outside the *virial cone* (circumscribing the virial sphere). Inside, the virial cone, the probability is obtained by comparing the predicted densities in PPS of the *halo* members (galaxies within the virial sphere) and the *interlopers* (galaxies within the virial cone, but outside the virial sphere). This can be written

$$p(R,v) = \begin{cases} \dfrac{g_{\rm h}(R,v)}{g_{\rm h}(R,v) + g_{\rm i}(R,v)} & R \leqslant r_{200} \\ \\ 0 & R > r_{200} \end{cases} \tag{8}$$

where $g_{\rm h}$ and $g_{\rm i}$ are the densities in PPS of the halo members and interlopers, respectively. In practice, since the computation of the first expression of equation (8) is limited to the galaxies within the virial cone, there are few galaxy distances to compute around each group centre.

(5a) *Halo density in projected phase space*
Given a galaxy number density profile $\nu(r)$, the density of halo particles in PPS is (following Mamon et al. 2013, replacing infinities by the virial radius):

$$g_{\rm h}(R,v) = \Sigma_{\rm sph}(R)\ \langle h(v|R,r)\rangle_{\rm LOS-sph} \,, \tag{9}$$

where $\Sigma_{\rm sph}$ is the surface density of the galaxies limited to the virial sphere:

$$\Sigma_{\rm sph}(R) = 2\int_R^{r_{200}} \nu(r)\,\frac{r\,{\rm d}r}{\sqrt{r^2 - R^2}} \,, \tag{10}$$

while $h(v|R,r)$ is the probability of having a LOS velocity v at the position in space given by (R,r), or when taking a LOS coordinate whose origin is at the group centre, at position $(R, z{=}\sqrt{r^2-R^2})$. Combining equations (9) and (10) one obtains

$$g_{\rm h}(R,v) = 2\int_R^{r_{200}} \nu(r)\,h(v|R,r)\,\frac{r\,{\rm d}r}{\sqrt{r^2 - R^2}} \,. \tag{11}$$

Assuming Gaussian (Maxwellian) three-dimensional velocities,[5] Mamon et al. (2013) have shown that the LOS velocity distribution at position (R,r) is also a Gaussian:

$$h(v|R,r) = \frac{1}{\sqrt{2\pi\sigma_z^2(R,r)}}\ \exp\left[-\frac{v^2}{2\,\sigma_z^2(R,r)}\right] \,, \tag{12}$$

with

$$\sigma_z^2(R,r) = \left(1 - \beta(r)\frac{R^2}{r^2}\right)\,\sigma_r^2(r) \,, \tag{13}$$

where $\beta = 1 - \sigma_\theta^2/\sigma_r^2$ is the velocity anisotropy (for radial velocity dispersion σ_r and one component of the tangential velocity dispersion σ_θ). In the presence of measurement errors of the LOS velocity, assumed Gaussian with zero bias and standard deviation $\epsilon(v)$, the new distribution of LOS velocities is the convolution of the zero-error $h(v|R,r)$ of equation (12) by a Gaussian

[5] It is easy to improve this model using the joint q-Gaussian (Tsallis) velocity dispersion that Beraldo e Silva et al. (2015) found to represent better the 3D velocity distribution in ΛCDM haloes.

of standard deviation $\epsilon(v)$. Then, in the expression of $h(v|R,r)$ (eq. [12]), the local LOS velocity variance σ_z^2 in equation (13) is replaced by $\sigma_z^2(R,r)+\epsilon^2(v)$. The radial velocity variance σ_r^2 in equation (13) is obtained (eq. [A1] in Appendix A) from the stationary spherical Jeans equation of local dynamical equilibrium

$$\frac{\mathrm{d}\left(\nu\sigma_r^2\right)}{\mathrm{d}r} + 2\,\beta(r)\,\frac{\nu\sigma_r^2}{r} = -\nu\frac{GM(r)}{r^2}\;, \tag{14}$$

where $M(r)$ is our chosen total mass profile.[6]

We assume that the galaxy distribution follows the mass distribution, and assume an NFW model for these two quantities. Denoting a the scale radius of the NFW density profile

$$\nu_{\rm NFW}(r) \propto \frac{1}{r\,(r+a)^2}\;,$$

(in the NFW model, a happens to be equal to the radius where the logarithmic slope of the density profile is equal to -2), we define the *concentration parameter* $c_{200} = r_{200}/a$. We adopt the scaling between r_{200} and $M_{200} = M(r_{200})$ from the measurements on ΛCDM haloes at $z = 0$ by Macciò et al. (2008). The NFW density profile can then be written

$$\nu(r) = \frac{N_{200}}{4\pi r_{200}^3}\,\widehat{\nu}\left(\frac{r}{r_{200}}\right)\;, \tag{15}$$

$$\widehat{\nu}(x) = \frac{1}{\ln(c_{200}+1)-c_{200}/(c_{200}+1)}\,\frac{x^{-1}}{(x+1/c)^2}\;, \tag{16}$$

where N_{200} is the number of predicted galaxies (above some minimum luminosity or stellar mass) within the virial sphere. We shall see, below, that the normalization N_{200} cancels from equation (8). The mass profile of the groups is

$$M(r) = M_{200}\,\frac{\ln(x+1)-x/(x+1)}{\ln(c_{200}+1)-c_{200}/(c_{200}+1)}\;, \tag{17}$$

where, again, $x = r/r_{200}$.

Finally, we adopt the velocity anisotropy profile that Mamon & Łokas (2005) found to represent well the particles in cluster-mass ΛCDM haloes

$$\beta(r) = \frac{1}{2}\,\frac{r}{r+r_\beta}\;, \tag{18}$$

with $r_\beta \simeq r_{200}/c_{200}$ (Mamon et al. 2010).

For our choice of NFW mass model and Mamon & Łokas anisotropy model, the radial velocity variance is given in equation (A2) of Appendix A.

(5b) *Interloper surface density in projected phase space*

Analyzing the distribution of dark matter particles within a hydrodynamical cosmological N-body simulation, Mamon et al. (2010) have found that the distribution of interlopers in PPS can be written as a Gaussian of the LOS velocity plus a constant term, where the coefficients of the Gaussian depend on projected radius:

$$g_{\rm i}(R,v) = \frac{N_{200}}{r_{200}^2 v_{200}}\,\widehat{g}_{\rm i}\left(\frac{R}{r_{200}},\frac{v}{v_{200}}\right)\;, \tag{19}$$

$$\widehat{g}_{\rm i}(X,u) = A(X)\,\exp\left[-\frac{1}{2}\,\frac{u^2}{\widehat{\sigma}_{\rm i}^2(X)}\right] + B, \tag{20}$$

[6] The general form of the Jeans equation in an expanding Universe contains extra terms that do not appear in our "standard" Jeans equation (14) for the density of the Universe, dark energy, streaming motions and non-stationarity (Falco et al. 2013). However, the solution of equation (A1) of the "standard" Jeans equation is a highly accurate solution of the "general" Jeans equation for $r < 2\,r_{100} \simeq 2.7 r_{200}$ (Falco et al. 2013).

where

$$A(X) = \mathrm{dex}\left(-1.061+0.364\,X^2-0.580\,X^4 +0.533\,X^6\right)\;, \tag{21}$$

$$\widehat{\sigma}_{\rm i}(X) = 0.612-0.0653\,X^2\;, \tag{22}$$

$$B = 0.0075\;, \tag{23}$$

where cosmic variance fluctuations are 0.11, 0.23 and 0.40 dex for $\widehat{\sigma}_{\rm i}(X)$, $A(X)$, and B, respectively (Mamon et al. 2010). The velocity v_{200} is the circular velocity at r_{200}, i.e. $v_{200} = 10\,H(z)\,r_{200}$. In the presence of velocity measurement errors of dispersion $\epsilon(v)$, one should replace $\widehat{\sigma}_{\rm i}^2$ by $\widehat{\sigma}_{\rm i}^2+\epsilon^2(v)/v_{200}^2$.

Since galaxies are somewhat biased tracers of the dark matter distribution, one needs to re-estimate the functions $A(X)$, $\sigma_{\rm i}(X)$, as well as B from a mock that is built from the galaxy distribution rather than the dark matter particles. In Appendix B, we present our analysis of the z=0 output of the SAM of Guo et al. (2011), deriving

$$\log_{10} A(X) = -1.092-0.01922\,X^3+0.1829\,X^6\;, \tag{24}$$

$$\sigma_{\rm i}(X) = 0.6695-0.1004\,X^2\;, \tag{25}$$

$$B = 0.0067\;. \tag{26}$$

We thus adopt, in this work, the functional fits provided in equations (24), (25), and (26), which admittedly are close to those of equations (21), (22), and (23).

Equations (19) – (23) depend little on halo mass in the cluster-mass regime (Mamon et al. 2010), and we assume here that these equations extend to group masses, in particular for the functional forms (eqs. [24]-26]) that we derived in Appendix B for the Guo et al. SAM.

We note that the normalization N_{200} appears in both $g_{\rm h}$ and $g_{\rm i}$, so it cancels out of the probability $p(R,v)$ of equation (8).

In our scheme, central galaxies have $R = 0$ and $v = 0$, by definition, and we set to unity their probability of membership (since the NFW central surface density diverges). To avoid too much group fragmentation, we do not assign a galaxy as a potential central group galaxy if it has a probability $p > p_{\rm cen}$ of belonging to another group of greater central galaxy stellar mass (since we proceed with groups of decreasing central galaxy stellar masses). Here, $p_{\rm cen}$ is a free parameter of MAGGIE. If $p_{\rm cen} = 1$, all galaxies can be group centres (case of maximum group fragmentation and no group merging). If $p_{\rm cen} = 0$, no satellite galaxy of a massive group can be the centre of another one (no group fragmentation, but maximal group merging). In other words, with $p_{\rm cen} = 0$, galaxies lying in the virial cone of a massive central galaxy, but far in the foreground/background, will be assigned membership probabilities to the group around this first galaxy, but will not be assigned membership probabilities to potential groups around potential central galaxies lying in the same virial cone. However, if the central galaxy of the first group was wrongly determined, then one can effectively have group fragmentation, even with $p_{\rm cen} = 0$ (but this occurs very rarely). Our tests showed that the performance of MAGGIE was independent of $p_{\rm cen}$ for $0 < p_{\rm cen} < 0.5$, and we adopted $p_{\rm cen} = 0.001$.

(6) *Group global properties*

The group global properties are obtained by using the galaxy membership probabilities as weights, i.e. group luminosities $L_{\rm group}$ and

stellar masses $m_{\rm group}$ are obtained with

$$L_{\rm group} = \sum_i p(R_i, v_i)\, L_i \ , \quad (27)$$

$$m_{\rm group} = \sum_i p(R_i, v_i)\, m_i \ . \quad (28)$$

over all galaxies with $p(R, v) \geqslant p_{\rm mem}$, where $p_{\rm mem}$ is another free parameter of MAGGIE. If $p_{\rm mem} = 1$, the group luminosities and stellar masses will correspond to the values of the central galaxies, while if $p_{\rm mem} = 0$, all galaxies within the virial cone will be considered when computing the luminosities and stellar masses, even those that contribute a tiny probability. Clearly, there should be little difference between setting $p_{\rm mem}$ = 0.001 or $p_{\rm mem} = 0$. But physically, galaxies with extremely low $p_{\rm mem}$ typically correspond to interlopers that are many group standard deviations in the foreground or background,[7] in projection and it makes little sense to keep them in the group. We thus choose to set $p_{\rm mem} = 0.001$.

(7) *Loop convergence*

We return to step (1), waiting for convergence when the number of groups found on the current pass matches the numbers found in the previous 3 passes. While the number of groups evolves towards a fixed value, it does not converge after 20 passes, hence we stop the iteration after the twentieth pass.[8]

Note that the central galaxy is in general the most luminous (MAGGIE-L) or the most massive in stars (MAGGIE-M). However, there are rare exceptions where a group may contain a galaxy that is more luminous or massive than its central, and yet is not the central of another previously found group, i.e. a group whose central is more luminous or massive.

2.2 Edge effects

Aside from all-sky surveys, galaxy surveys have edges on the sky. Moreover, all volume-limited subsamples of galaxy surveys (including all-sky) will have edges in redshift space. Galaxy groups lying too close to an edge may be truncated. The grouping algorithm may detect the truncated group without knowing how much of the group lies beyond the survey edge. There is therefore no simple recipe to handle survey edges.

For groups lying near a survey edge, following Yang et al. (2007) we generate 700 galaxies (Yang et al. use 200) following the NFW profile, using the halo concentration estimated by the halo mass from Macciò et al. (2008). Then, we project galaxies on the celestial sphere and we estimate the number of galaxies weighted by their probabilities that fall outside the galaxy survey zone. For this, we also need to generate galaxy velocities. We assume that the 3D velocity distribution is Maxwellian and that the velocity anisotropy is that given by Mamon & Łokas (2005). Next, we compute the fraction of galaxies that are outside the survey (still weighted by galaxy probabilities) and then the total stellar mass and luminosity of the group are corrected by dividing by this fraction (see Yang et al. 2007). Admittedly, if a large group is centered just beyond the survey edge, only a small fraction of this group will intersect our survey mask, so we will underestimate its virial radius and mass.

[7] Groups lying very close to the virial cone also have very low membership probabilities.

[8] The number of groups oscillates around a value, but in an aperiodic fashion.

Table 1. Doubly complete subsamples of the mock SDSS/Legacy survey.

Subsample	$z_{\rm min}$	$z_{\rm max}$	$M_r^{\rm max}$	$L_{\rm min}/L*$	galaxies
Nearby	0.01	0.053	–19.0	0.14	72 510
Distant	0.01	0.102	–20.5	0.56	213 546

3 TESTS OF MAGGIE ON MOCK CATALOGUES

We test MAGGIE using realistic mock, doubly complete in distance and luminosity, galaxy redshift catalogues, which we had previously used in Paper I to optimize the FoF linking lengths. The construction of the mock catalogues and the description of the tests are discussed in detail in Paper I, and are briefly recalled below.

3.1 Mock galaxy sample

We have constructed a mock galaxy catalogue corresponding to the extent on the sky and depth of the largest contiguous (2.2 sr) region of the primary (Legacy) spectroscopic sample of the SDSS. For this, we replicated the galaxy outputs at $z = 0$ generated from the Guo et al. (2011) semi-analytical model (SAM) of galaxy formation and evolution, which was run on the halo merger trees extracted from the Millennium-II dissipationless cosmological N-body simulation (Boylan-Kolchin et al. 2009), which itself had been run in a box of comoving size $L_{\rm box} = 100\ h^{-1}{\rm Mpc}$, with cosmological parameters $\Omega_m = 0.25$, $\Omega_\Lambda = 0.75$, $H_0 = 73$ and $\sigma_8 = 0.9$, and particle mass $1.1 \times 10^7 {\rm M}_\odot$. Haloes were identified by applying the Friends-of-Friends (FoF) technique to the real space particle data.

In the output of the Guo et al. SAM, each galaxy is associated to a halo, making it easy to compare the groups extracted from our algorithm to the real space groups. Guo et al. found that the z=0 galaxy luminosity and stellar mass functions agree well with the corresponding observed functions, making their galaxy catalogue realistic and useful to test our algorithm on data similar to observations.

The maximal redshift spanned by the simulation box is approximately $H_0 L_{\rm box}/c \approx 0.025$. Simulating the SDSS survey requires a deeper sample (see Table 1). For this, we have juxtaposed several boxes of the galaxy catalogue, applying random translations and rotations in galaxies coordinates to avoid perspective effects (Blaizot et al. 2005). This produced a larger *superbox* composed of the replicas of the galaxies in the computation box. We placed the observer at the middle of one of the sides of the superbox (see Fig. 1 of Paper I). Redshifts of the galaxies were computed using velocities given in the galaxy catalogue and adding the Hubble flow to it (see Paper I).

Our mock survey had no holes caused by saturated stars or bad data. Nevertheless, we allowed for observational errors on galaxy luminosities and stellar masses. According to Appendix C1, the errors on galaxy stellar masses, determined by comparison of different stellar mass algorithms on hundreds of thousands of SDSS galaxies, are roughly 0.2 dex. This value is much more conservative than the value of 0.10 dex (Taylor et al. 2011), and 0.15 dex (Mendel et al. 2014), but consistent with the 95% confidence errors of 0.30 and 0.35 dex for blue and red galaxies, as deduced by Conroy et al. (2009). In Appendix C2, we estimate the errors on galaxy luminosities, taking into account errors in photometry and redshift, uncertainties on extinction corrections and k-corrections, and neglect of peculiar velocities. We find that the errors on galaxy luminosities are of order of 0.08 dex at our minimum redshift of

$z = 0.01$ decreasing to 0.06 dex at our maximum redshift of $z \simeq 0.1$. In our analysis, we have therefore generated Gaussian errors without bias and with dispersion of 0.2 dex for log stellar masses and 0.08 dex for log luminosities.

From our flux-limited mock galaxy survey, we constructed several subsamples that are doubly complete in distance and luminosity. We focus our results on the two subsamples shown in Table 1.

3.2 Flags

We flagged all galaxies belonging to real-space FoF groups containing at least one member that was on the other side of the periodic box (their groups would thus be split by the transformations of the box).

We also flagged the galaxies in the extracted groups that lie close to the redshift space edges of the doubly complete subsamples: to be very conservative, we flagged all extracted groups lying closer (roughly 2.5 Mpc) to the angular edges than would be the virial radius of a massive ($\log_{10} M = 15.2$) cluster, and all groups lying closer to the redshift limits than 13 times this distance (see Mamon et al. 2010) to account for redshift distortions.[9]

We ran MAGGIE on all galaxies of the mock (flagged or unflagged), and subsequently flag the groups that contain at least one flagged galaxy with $p > p_{\rm mem}$.

3.3 Testing procedures

Following Paper I, we applied a suite of tests to groups containing no flagged galaxies to assess the performance of MAGGIE, its robustness to some of the assumptions, and to compare it to other group finders.The tests check how well the sample of *extracted groups* in redshift space (hereafter, EGs) matches the sample of *true groups* in real space (hereafter, TGs). The TGs are defined as the set of galaxies that lie within the virial sphere around the centre of the real space group, i.e. the position of the most bound particle of the halo (Boylan-Kolchin et al. 2009).

In an optimal grouping algorithm, the TGs minimally suffer from *fragmentation* into several EGs. A fragmented TG contains the central galaxies (see beginning of Sect. 2.1) of several EGs. There should also be minimal *merging* of several TGs into a unique EG (the EG contains the central galaxies of several TGs, each with $p \geqslant p_{\rm mem}$). Following Yang et al. (2007) and Paper I, the EGs and TGs are linked by their respective central galaxies. When fragmentation occurs, the primary EG is that containing the central galaxy of the parent TG. When merging occurs, the primary TG is that containing the central galaxy of the EG. We refer the reader to fig. 3 of Paper I for illustrations of group fragmentation and merging.

Also, in the optimal grouping algorithm, the galaxies of the EG should represent a maximally *complete* sample of the parent TG galaxies, and a maximally *reliable* (pure) sample, i.e. with as high as possible fraction of galaxies that belong to the parent TG (recall that the TG is the set of galaxies within the virial sphere).

Finally, the optimal grouping algorithm should produce EG luminosities, stellar masses and total masses as close as possible to those of the parent TG, i.e. with minimal *bias* and *scatter*. While bias can be corrected for, a measurement with strong scatter will be *inefficient*.

[9] The number of unflagged galaxies depends on the group finder and the subsample.

When TGs are fragmented, it makes little sense to measure the reliability of the galaxy membership of the secondary EGs (secondary fragments), and when TGs are merged, it would similarly not be useful to measure the completeness of the galaxy membership of a secondary TG. And it only makes sense to compare EG properties with the corresponding TG ones for primary fragments or relative to primary parent TGs. So all measures of completeness, reliability, as well as bias and scatter of group luminosity, stellar and total masses are limited to the primary EGs. The reader is referred to Paper I for more details.

Since the galaxy membership of MAGGIE groups is probabilistic, some of the statistical tests must be modified. In Paper I, we defined the galaxy reliability as[10]

$$R = \frac{\rm TG \cap EG}{\rm EG} = \frac{N_{i\in {\rm TG}\cap {\rm EG}}}{N_{i\in {\rm EG}}} \,, \tag{29}$$

where we adopt the notation $N_{i\in\mathcal{E}}$ to represent the number of elements in space $\mathcal{E}$. For our probabilistic MAGGIE group finder, we modify equation (29) to

$$R = \frac{\rm TG \cap EG}{\rm EG} = \frac{\sum_{i\in {\rm TG}\cap {\rm EG}} p_i}{\sum_{i\in {\rm EG}} p_i} \,, \tag{30}$$

where $p_i \equiv p(R_i, v_i)$ is the probability of membership of galaxy i (eq. [8]). The equivalent of equation (30) for the completeness would be

$$C = \frac{\rm TG \cap EG}{\rm TG} = \frac{\sum_{i\in {\rm TG}\cap {\rm EG}} p_i}{N_{i\in {\rm TG}}} \,. \tag{31}$$

However, it is inconsistent to consider probabilities in the numerator of equation (31) and not in its denominator. We therefore adopt instead a definition based on hard assignments:

$$C = \frac{\rm TG \cap EG}{\rm TG} = \frac{N_{i\in {\rm TG}\cap {\rm EG} \ {\rm AND} \ p_i > p_{\rm mem}}}{N_{i\in {\rm TG}}} \,. \tag{32}$$

Since our chosen value of $p_{\rm mem}$ is very small, the definition of completeness in equation (32) is very close to the definition of paper I

For group luminosities and stellar masses, we use the probabilities as in equations (27) and (28), respectively.

Finally, we did not measure group merging in this work. The logical way of estimating group merging is to request that two TG centrals are members of the same EG. But with a probabilistic method such as MAGGIE, a given galaxy may be a member of several EGs (with different membership probabilities in each, all with $p > p_{\rm cen}$). So it is not clear a group merger occurs when one of the TG centrals is a member of 2 EGs, with a much lower probability of membership in the EG that contains the central of the other TG compared to the probability of membership in the other EG.

4 RESULTS

We now present the results of our tests on group fragmentation, galaxy completeness and reliability, accuracies of group total masses, luminosities and stellar masses. We ran these tests on both MAGGIE-L and MAGGIE-M, using mocks without or with the inclusion observational errors of 0.08 dex in luminosity and 0.2 dex in

[10] Note that our *reliability*, which can take values in the range $[0-1]$, is different from the *purity* used by Yang et al. (2007) and Domínguez Romero et al. (2012), defined as TG/EG=R/C, and also different from one minus their *contamination*, defined as (EG–TG∩EG)/TG=$C(1/R–1)$, which both can be greater or smaller than unity.

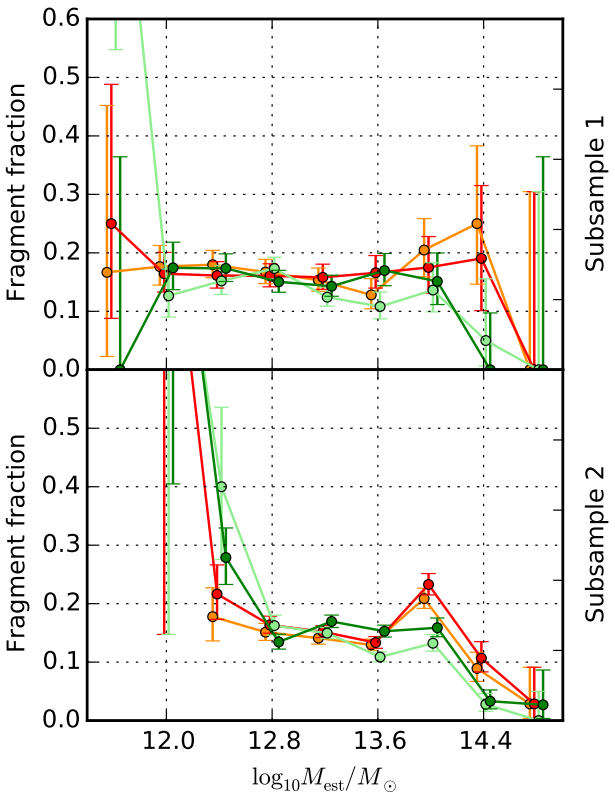

Figure 1. Fraction of extracted groups that are secondary fragments as a function of their estimated group mass, for unflagged groups of at least 3 members (for both the extracted and true groups), for both the nearby (*top*) and distant (*bottom*) subsamples. The line colours are *dark green* and *red* for MAGGIE-M and MAGGIE-L, with respective observational errors of 0.2 dex on stellar mass and 0.08 dex on luminosity, and *light green* and *orange* for MAGGIE-M and MAGGIE-L, with zero observational errors. The error bars are computed with the Wilson (1927) formula (see text). The points have their abscissa slightly shifted for clarity.

stellar masses. We, however, defer the discussion of the impact of observational errors to Sect. 5.2.

4.1 Fragmentation

Figure 1 displays the fraction of extracted groups (EGs) that are secondary fragments as a function of estimated group mass. The error bars are obtained with the Wilson (1927) formula.[11] Both versions of MAGGIE lead to fragmentation of typically 15%, even when realistic errors on galaxy luminosities and stellar masses are considered. The fragmentation in MAGGIE is fairly independent of the chosen doubly complete subsample, except that extracted groups with low estimated masses ($\log M_{\rm est}/{\rm M}_\odot < 12.5$) are more likely to be secondary fragments when in the distant subsample, where most of the groups lie too far to permit the detection of such low mass groups. In the high-mass end, one finds that the MAGGIE-M EGs are less likely to be secondary fragments than their MAGGIE-L counterparts.

[11] The Wilson (1927) formula avoids zero errors when the fraction is zero or unity. It is described in the Wikipedia entry Binomial proportion confidence interval, http://en.wikipedia.org/wiki/Binomial_proportion_confidence_interval.

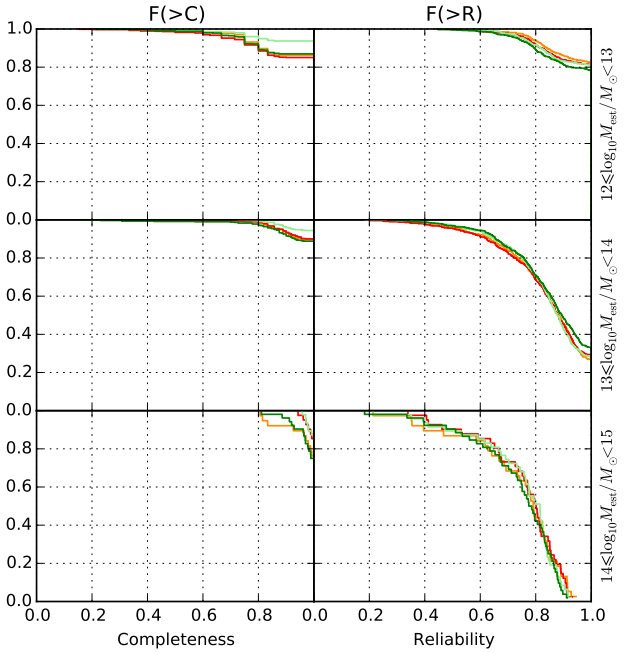

Figure 2. Cumulative distribution functions of the galaxy membership completeness (*left*, computed with eq. [32]) and reliability (*right*, both relative to the virial sphere of the true groups, computed with eq. [30]) in bins of estimated group masses, for the nearby subsample (unflagged galaxies in groups of at least 3 true and 3 extracted members that are not secondary fragments). The colours are the same as in Figure 1.

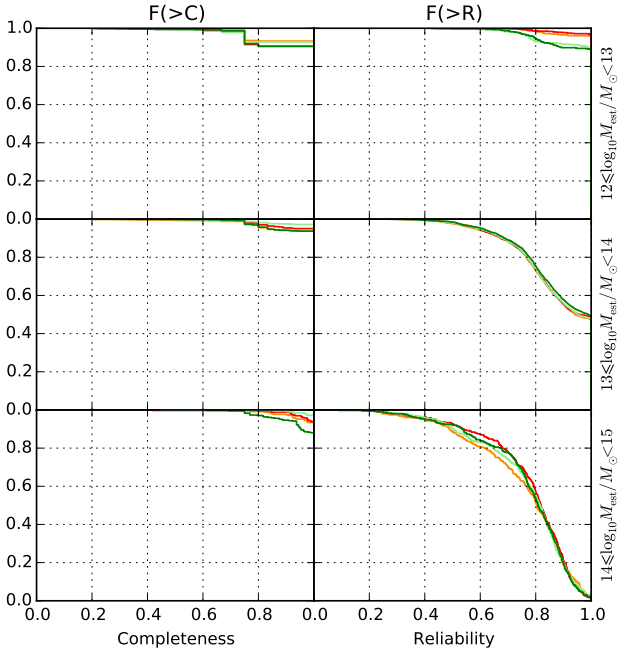

Figure 3. Same as Figure 2, but for the distant subsample.

4.2 Completeness and reliability

Figures 2 and 3 show that the EGs from MAGGIE-M (dark green lines) and MAGGIE-L (red lines) that are primary fragments are highly complete in galaxies. For the nearby subsample (Fig. 2), in the worst performing among MAGGIE-M and MAGGIE-L, with ob-

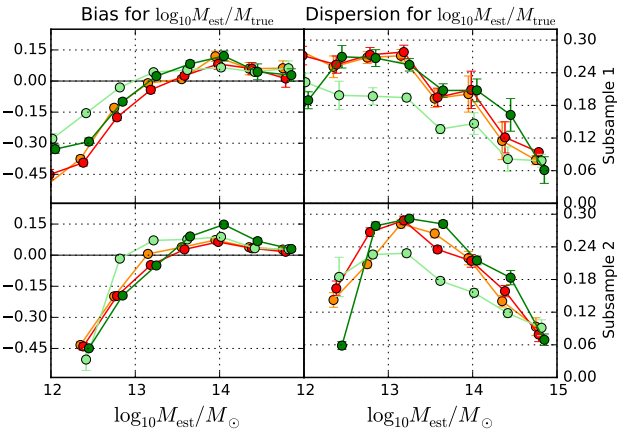

Figure 4. Median bias and scatter (using 16th and 84th percentiles) of extracted group total mass within the virial sphere (for unflagged primary groups of at least 3 true and 3 extracted galaxies), for the nearby (*top*) and distant (*bottom*) subsamples. The error bars for the bias and scatter are respectively $\sigma/\sqrt{N}$ and $\sigma/2\,[2/(N-1)+\kappa/N]^{1/2}$, where κ is the kurtosis excess. The points have their abscissa slightly shifted for clarity. Same colours as Figures 1 and 15.

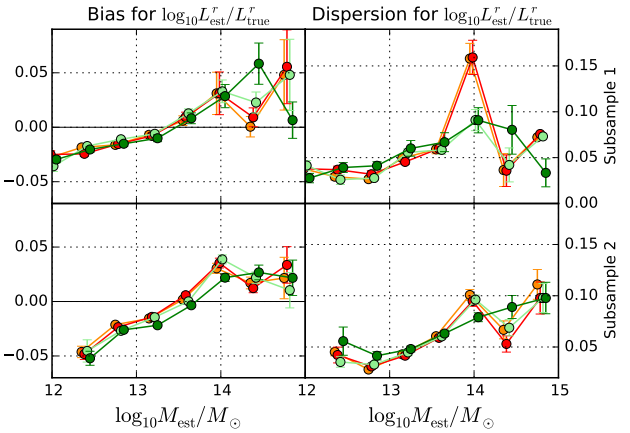

Figure 5. Median bias and scatter (using 16th and 84th percentiles) of extracted group r-band luminosity within the virial sphere (for unflagged primary groups of at least 3 true and 3 extracted galaxies). The points have their abscissa slightly shifted for clarity. Same colours as Figures 1 and 15.

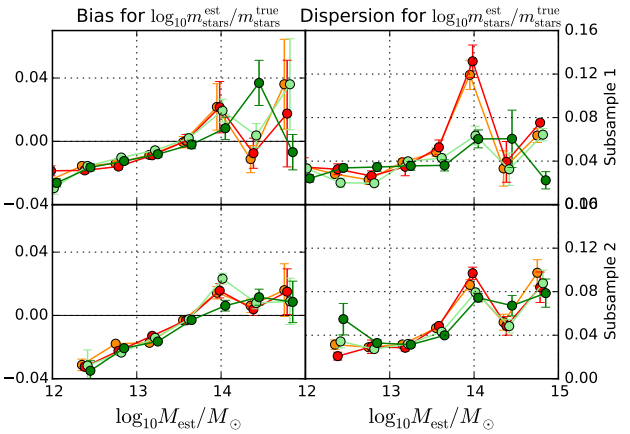

Figure 6. Same as Figure 5, but for group stellar mass.

servational errors, 100% completeness is achieved for 85%, 89% and 75% of the groups, for the low, intermediate and high mass bins, respectively, and 90% completeness is reached for 90%, 93% and 95% of the groups in the same respective mass bins. The completeness is even higher for the distant subsample (Fig. 3). The galaxy completeness values are roughly the same with MAGGIE-L and MAGGIE-M, except for the high-mass end where MAGGIE-L shows higher completeness.

The galaxy reliability of MAGGIE decreases with increasing EG mass: For the worst performing among MAGGIE-M and MAGGIE-L with observational errors, the fractions of 90%-reliable groups are respectively 82%, 43%, and 4% for the nearby subsample. The median galaxy reliabilities for the high-mass bin are more similar: while they are respectively 80% and 82% (78% and 81%) with MAGGIE-L (MAGGIE-M), again with observational errors. The galaxy reliabilities are very similar between MAGGIE-L and MAGGIE-M, except that MAGGIE-L shows higher reliability in the low mass bin of the distant subsample.

4.3 Accuracy in group total masses

Figure 4 shows the bias and scatter in group mass. Both flavours of MAGGIE, without or with errors, have their group masses biased low at low masses, by typically 0.4 dex at $\log M_{\rm est}/{\rm M}_\odot = 12.5$. The estimated masses are unbiased at $\log M_{\rm est}/{\rm M}_\odot \approx 13.5$ and are slightly positively biased at high mass, especially at $\log M_{\rm est}/{\rm M}_\odot \approx 14$, where the bias reaches ≈ 0.1 dex. The bias is never more than 0.1 dex in absolute value for groups with $\log M_{\rm est}/{\rm M}_\odot > 12.8$. There are no significant differences in group total mass bias between MAGGIE-L and MAGGIE-M.

While bias can be corrected for, scatter is a more serious concern. The dispersion in $M_{\rm est}/M_{\rm true}$ decreases with EG mass, from typically 0.2 dex at $\log M_{\rm est}/{\rm M}_\odot = 12$ to 13 to better than 0.1 dex at $\log M_{\rm est}/{\rm M}_\odot = 14.8$.

4.4 Accuracy in group luminosities and stellar masses

Figures 5 and 6 show the bias and inefficiency of the recovered group luminosities and stellar masses, respectively (using eqs. [27] and [28]). MAGGIE groups with low estimated total masses are slightly biased low, by up to typically 0.03 dex (7%) at $\log M_{\rm est}/{\rm M}_\odot = 12$ (but 0.05 dex for group luminosities in the distant subsample). At high estimated group masses, the bias is less well measured (given the lower number of groups in the higher mass bins), and some fluctuations appear, but the overestimate of the group total masses is typically limited to 0.04 dex (10%). There are virtually no differences in the luminosity and stellar mass biases between MAGGIE-L and MAGGIE-M.

Surprisingly, the inefficiencies in group luminosity or stellar mass estimation with both flavours of MAGGIE increase with EG mass, typically from 0.03 or 0.04 dex in the low EG mass end to 0.05 dex at the high end (0.08 dex for the distant subsample). MAGGIE-L and MAGGIE-M have comparable dispersions in luminosity and stellar mass, except that MAGGIE-L is worse in one mass bin ($M_{\rm est}/{\rm M}_\odot \approx 14$), but this bad performance of MAGGIE-L in a single mass bin might be of statistical nature.

5 DISCUSSION

Our tests have been performed in an idealized situation for MAGGIE, with perfectly known scaling relations, yet with realistic measurement errors on galaxy luminosities and stellar masses. We now discuss the general features of MAGGIE (Sect. 5.1), and then the performance of MAGGIE in terms of its sensitivity to observational errors (Sect. 5.2), and its robustness relative to the adopted initial mass – luminosity scaling relation (Sect. 5.3.1), the HMF (Sect. 5.3.2), cosmological parameters (Sect. 5.3.3), and the precise choice for the density of interlopers in PPS, $g_{\rm i}(R, v)$ (Sect. 5.3.4), before comparing its performances in Sect. 5.4 to two popular group finders: FoF and the halo-based group-finder of Yang et al. (2005, 2007).

5.1 General features of MAGGIE

Thanks to its probabilistic nature, MAGGIE generally performs well with galaxy membership reliability, since the least reliable galaxies along the LOS are assigned low probabilities. In general, extracted global properties of groups should be less biased and errors in membership are usually tempered by the low probabilities assigned to uncertain members.

Since at high group (halo) mass, group luminosity and stellar mass are less sensitive to group (halo) mass (Marinoni & Hudson 2002), the group mass that is obtained with the AM technique is more sensitive to the observable group luminosity or stellar mass. Moreover, high-mass groups (clusters), which are known to have a more prominent Red Sequence of galaxies, should have higher stellar mass to luminosity ratios. This means that, measuring group mass with AM will be more accurate using group stellar masses than with group luminosities. This is, indeed, what is seen (Fig. 4) in our tests of the accuracies of MAGGIE group total masses without observational errors, as MAGGIE-M (light green) masses are significantly more accurate than those of MAGGIE-L (orange). But the greater observational errors on stellar masses relative to luminosities reverse this hierarchy, making MAGGIE-L slightly more accurate than MAGGIE-M. in extracting group total masses.

MAGGIE assigns non-zero probabilities to all galaxies lying within the virial cone, and only considers those for which $p > p_{\rm mem} = 0.001$. If the virial radius is overestimated, MAGGIE will be more prone to group merging and the galaxy membership will be less reliable. The bloated sizes of high-mass groups, as witnessed by the mass bias going from negative to positive for MAGGIE groups (left panels of Fig. 4), explains the strong decrease in reliability with increasing estimated group mass (Figs. 2 and 3), especially in MAGGIE.

5.2 Robustness of MAGGIE to observational errors

While geometric based algorithms such as FoF or Voronoi-Delaunay methods are relatively immune to observational errors on luminosities and stellar masses, such errors can affect group finders that derive group total masses by AM with group luminosities or stellar masses, as those of Yang et al. (2007), Muñoz-Cuartas & Müller (2012), Domínguez Romero et al. (2012) and MAGGIE.

We have run MAGGIE both with and without the observational errors on galaxy luminosities and stellar masses. Figures 1–6 show the effects of going from no observational errors (orange for MAGGIE-L and light green for MAGGIE-M) to realistic observational errors (red for MAGGIE-L and green for MAGGIE-M).

Including observational errors produces only small extra group fragmentation, by typically 10 percent for MAGGIE-L and 20 percent MAGGIE-M, both in relative terms (Fig. 1).

Using the Kolmogorov-Smirnov (KS) test, we see (Figs. 2 and 3) that the observational errors significantly worsen the galaxy completeness of MAGGIE-M for low mass EGs of the nearby subsample (and marginally so for the intermediate and high mass EGs of the distant subsample), while MAGGIE-L does not seem affected. Neither MAGGIE-L nor MAGGIE-M see their galaxy reliability affected by the observational errors.

The inefficiency of group mass estimation is significantly worsened by the observational errors for MAGGIE-M (at virtually all EG masses), but not for MAGGIE-L (Fig. 4). While, with mocks that do not include observational errors, MAGGIE-M produces significantly more accurate group total mass estimation than does MAGGIE-L, the inclusion of observational errors inverses this hierarchy, with MAGGIE-L producing slightly more accurate group masses.

On the other hand, observational errors do not worsen the inefficiency of the estimation of group luminosities (Fig. 5) and stellar masses with either flavour of MAGGIE (Fig. 6).

5.3 Robustness of MAGGIE to details of the model

5.3.1 Initial halo mass – central stellar mass relation

We tested how MAGGIE is affected by our initial relation between halo mass and central stellar mass (item 2a of Sect. 2.1). We found that MAGGIE is insensitive to our adopted scheme of relating luminosity or stellar mass to halo mass in its first pass: the final variation of group M/L_r vs. L_r is precisely the same whether one adopts $M/L_r = 300$ or the relation of M/L_r vs. L_r that Behroozi et al. (2010) derived from AM. The same effect has been previously noticed by Yang et al. (2007).

5.3.2 Halo mass function model

The estimation of the virial mass (or virial radius) is a crucial step (item 2 in Sect. 2.1) of MAGGIE (and of other methods that use priors such as Yang et al. 2007 and Domínguez Romero et al. 2012). A biased estimate of group masses will affect the observed trends of galaxy properties with the global environment. The AM technique, used in MAGGIE (as well as by Yang et al., Muñoz-Cuartas & Müller 2012 and Domínguez Romero et al.) appears to be a good way to estimate the virial mass of galaxy group haloes. There are, however, three issues that need to be considered.

First, there may be haloes with no galaxies that may perturb the halo-group bijectivity assumption of AM. We checked that no haloes above $10^{11}{\rm M}_\odot$ in the Millennium-II simulation have zero galaxies assigned to them in the SAM of Guo et al. (2011).

Secondly, deriving group total masses by AM between an HMF and the inferred distribution of group galaxy luminosities or stellar masses should cause inefficient estimation of group masses when these are in the high range ($14 < \log_{10} M_{\rm est}/{\rm M}_\odot < 15$), because of the lower slope of the high mass end of the group luminosity (or stellar mass) as a function of halo mass at high halo mass (e.g., Yang et al. 2008, 2009).[12]

Thirdly, most analytical HMFs described in the literature are

[12] This issue is much more severe when one uses central galaxy (instead of group) luminosity or stellar mass (e.g., Yang et al. 2008, 2009; Cattaneo et al. 2011; Wojtak & Mamon 2013).

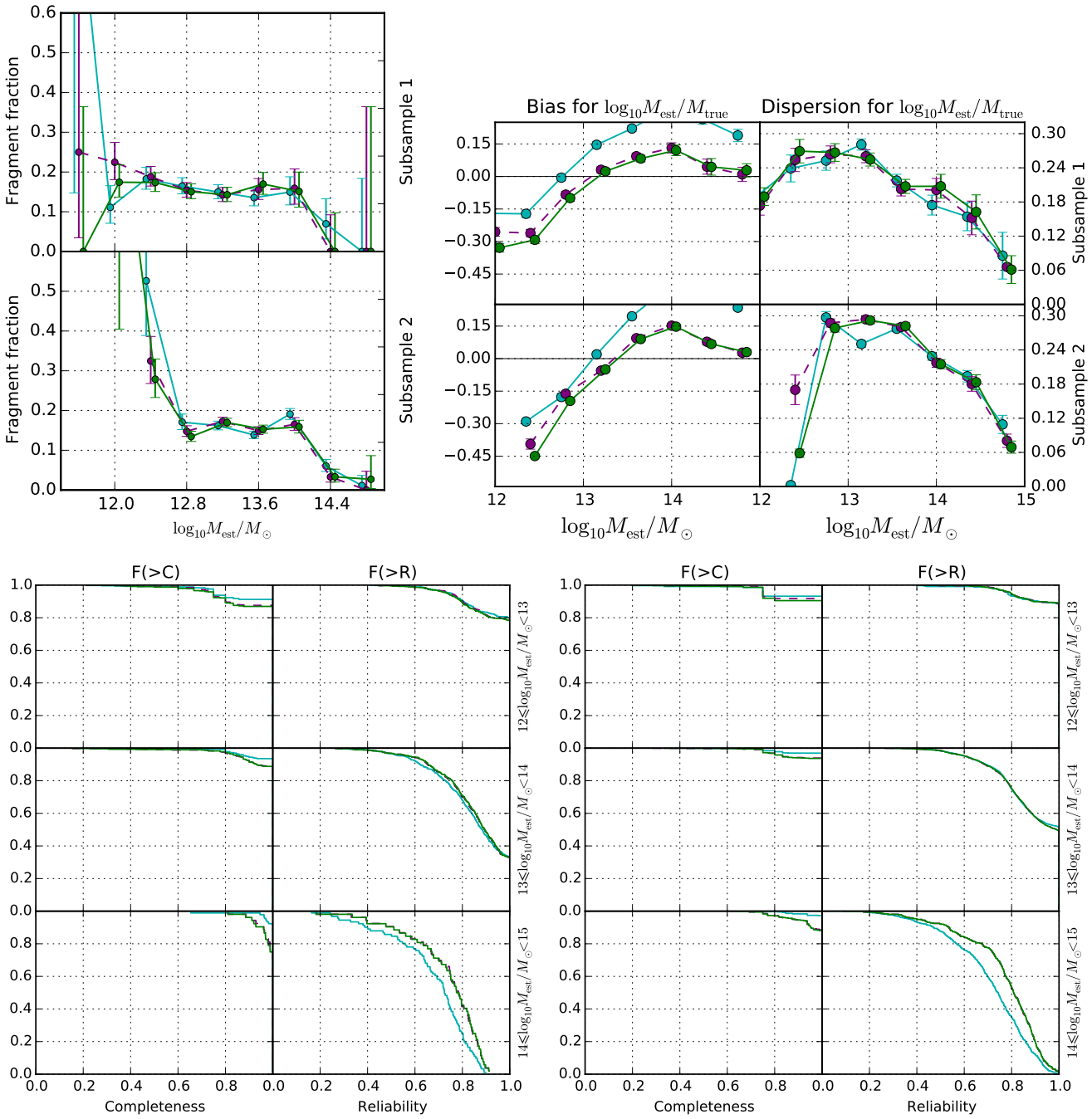

Figure 8. Effects of the choice of halo mass function on the fraction of fragments (*top left*), the accuracy in the recovered halo mass (*top right*), and the cumulative distribution functions of galaxy completeness and reliability of the groups (*bottom*) for MAGGIE-M (with 0.2 dex observational errors). The lines show the three adopted halo mass functions: our fit to the halo virial mass function (*green*, as used throughout article), and the analytical halo mass functions of Tinker et al. (2008, virial *purple, dashed*, for overdensity 800 relative to the mean, corresponding to 200 relative to critical for the cosmology of our mock) and Courtin et al. (2011, FoF, *light blue*). The analysis is for unflagged groups of at least 3 true and 3 extracted members. The points in the upper plots have their abscissa slightly shifted for clarity. The Tinker et al. lines are usually indistinguishable from those obtained with our fit.

based on fits to the FoF mass of the haloes instead of the spherical over-density mass, which is how we defined the virial mass of the halo. Since we used the galaxy catalogue from Guo et al. (2011), whose SAM was applied onto the Millennium-II run, we fit the halo *virial* mass function directly on its output.

Figure 7 shows the cumulative HMF computed in various ways. The figure clearly shows that the cumulative FoF HMF computed from the Millennium-II Simulation is typically 0.2 dex above the cumulative virial mass function computed from the same simulation. While the analytical approximation of Courtin et al. (2011, light blue) matches very well the halo FoF mass function,[13] Figure 7 shows that the cumulative halo virial mass function obtained

[13] Other analytical forms of the halo FoF mass function by Jenkins et al.

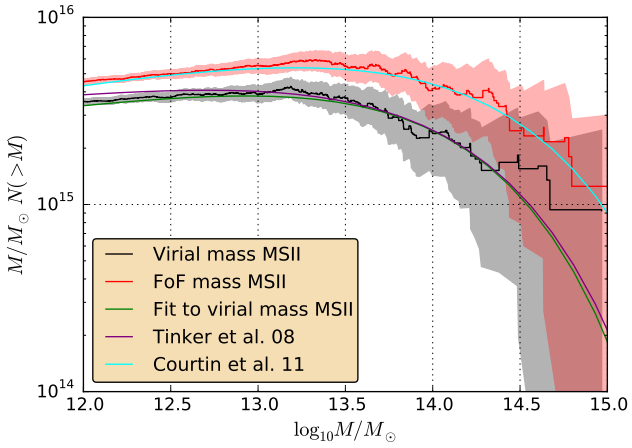

Figure 7. Cumulative z=0 halo mass functions (multiplied by halo mass for clarity) for the output of the Millennium-II simulation for FoF masses (*red*) and virial masses (M_{200}, i.e. computed in the sphere whose mean density is 200 times the critical density of the Universe, *black*), as well as the analytical forms from Courtin et al. (2011) for the halo FoF mass function (*cyan*) and from Tinker et al. (2008) for the halo mass function where the masses are in the spheres of overdensity of 800 relative to the mean density of the Universe (*purple*, corresponding to 200 times the critical density for $\Omega_{\rm m} = 0.25$ as in the Millennium Simulation). Also shown is our maximum likelihood fit to the virial mass function (*green*).

from the analytical approximation of Tinker et al. (2008, purple) is slightly offset, at low masses, relative to cumulative halo virial mass function extracted from the Millennium-II simulation.

We therefore chose, in our present tests, to fit ourselves the halo virial mass function of the Millennium-II simulation with the Tinker et al. (2008) model. Our maximum likelihood fit of the Tinker et al. function to the set of halo masses (green curve) produces Tinker et al. parameters $a = 2.13$, $b = 1.97$, and $c = 1.75$, with normalization $A = 0.188$ (instead of the corresponding values of $a = 1.87$, $b = 1.59$, $c = 1.58$, and $A = 0.248$ that Tinker et al. found for $\Delta_{\rm m} = 800$, i.e. $\Delta = 200$ given $\Omega_{\rm m} = 0.25$ of the Millennium-II simulation, purple curves).[14]

Figure 8 shows how the performance of MAGGIE is affected by the choice of HMF, respectively for group fragmentation, as well as the mass accuracy, galaxy completeness and reliability of the primary groups.

All three HMFs lead to similar group fragmentation, group total mass inefficiency and galaxy incompleteness. However, adopting the analytical approximation (by Courtin et al. 2011) to the halo FoF mass function (light blue lines and symbols) leads to significantly positive mass bias (up to 0.3 dex) at high EG masses (upper right plot of Fig. 8, and lower reliability at high EG masses (bottom plots of Fig. 8, only significant for the distant subsample according to our KS tests).

Substituting the HMF of Tinker et al. (2008), for overdensity 800 relative to the mean density of the Universe (corresponding to 200 times the critical density for the value of the cosmological density parameter used in the Millennium Simulation II, on which the galaxies of our mock were modeled with the SAM of Guo et al. 2011) yields very similar results to our standard HMF (which, we recall, is a fit of the Tinker et al. form to the halo mass distribution): these two HMFs (purple lines and symbols for the Tinker et al. HMF, green ones for our HMF) often lead to indistinguishable positions in the various plots of Figure 8 (recall that the points have their abscissa slightly shifted for clarity). This similarity reflects the similar HMFs seen in Figure 7 (purple vs. green curves). This suggests that one can use the Tinker et al. analytical fits to the halo virial mass function for the AM in MAGGIE.

5.3.3 *Cosmological parameters*

Groups extracted from group finders will depend on the choice of cosmological parameters. For example, when computing the projected radius of a galaxy at the redshift of the group, we implicitly need to compute the cosmological angular distance, $d_{\rm A}(z) = d_{\rm L}(z)/(1+z)^2$, hence the luminosity distance, $d_{\rm L}(z)$, which scales as the inverse dimensionless Hubble parameter, $1/h = 100\,{\rm km\,s^{-1}\,Mpc^{-1}}/H_0$, but also more subtly on $\Omega_{\rm m}$ and Ω_Λ. For our assumed flat ΛCDM Universe, the cosmological parameters reduce to h and $\Omega_{\rm m}$, and the luminosity distance is computed using elliptic integrals (Liu et al. 2011; see also Eisenstein 1997). Moreover, for all analytical HMFs tested in Sect. 5.3.2, we have assumed the same cosmological parameters as in our mock, i.e. those of the Millennium-II simulation, on which the galaxy SAM output was constructed, which in turn was used to build our mock redshift space survey. However, the observer may choose a different set of cosmological parameters.

We tested the sensitivity of MAGGIE to the choice of cosmological parameters, by comparing the results of MAGGIE-M (with observational errors) with the "true" cosmology ($\Omega_{\rm m} = 0.25, h = 0.73$ as assumed in the Millennium-II simulation, on which our mock is based) with analogous runs of MAGGIE-M assuming instead two "false" cosmologies (i.e. inconsistent with our mock): WMAP9, with $\Omega = 0.279, h = 0.70$ (Bennett et al. 2013) and Planck-2015 with $\Omega_{\rm m} = 0.308, h = 0.678$ (Planck Collaboration et al. 2015).

As seen in the plots of Figure 9, the choice of cosmological parameters affects very little the performance of MAGGIE-M on the fraction of groups that are secondary fragments (upper left plot), the inefficiency of group total mass estimation (right panels of upper right plot), as well as galaxy completeness, and accuracy in total group mass, with no statistically significant trends with $\Omega_{\rm m}$.

However, with Planck (royal blue), the galaxy reliability is significantly less reliable for the high EG mass bin of the distant sample (right panel of lower right plot of Fig. 9, again using a KS test) than when the mock cosmology is assumed (green).

Moreover, assuming WMAP9 (magenta) and especially Planck-2015 (royal blue) cosmologies leads to increasingly positive biases in group total mass (left panels of upper right plot) at the high EG mass end up to 0.15 dex higher (Planck) than with the cosmology of our mock (green). Indeed, the lower Hubble constants of the WMAP and especially Planck cosmologies, relative to the value used in the Millennium-II simulation, hence in our

(2001), Warren et al. (2006), and Crocce et al. (2010) are virtually identical to that of Courtin et al. (2011).

[14] Our fit is performed in the mass range $11 < \log M/{\rm M}_\odot < 15.5$. Following Jenkins et al. (2001), Tinker et al. (2008) fit a simple form for $f(\sigma) = (M/\overline{\rho})\,{\rm d}n/{\rm d}M\,/\,({\rm d}\ln\sigma^{-1}/{\rm d}\ln M)$, where σ is the standard deviation of primordial perturbations of mass M (linearly extrapolated to $z = 0$). The expression $f(\sigma)$ turns out to be only very weakly sensitive to the cosmological parameters and fairly weakly sensitive to redshift (Jenkins et al. 2001). However, the cumulative HMF of the Jenkins/Tinker model cannot be expressed in analytical form. Therefore, the normalisation of the probability density function of the halo mass distribution (required for the maximum likelihood estimate) requires in turn the numerical integration of the unnormalized HMF.

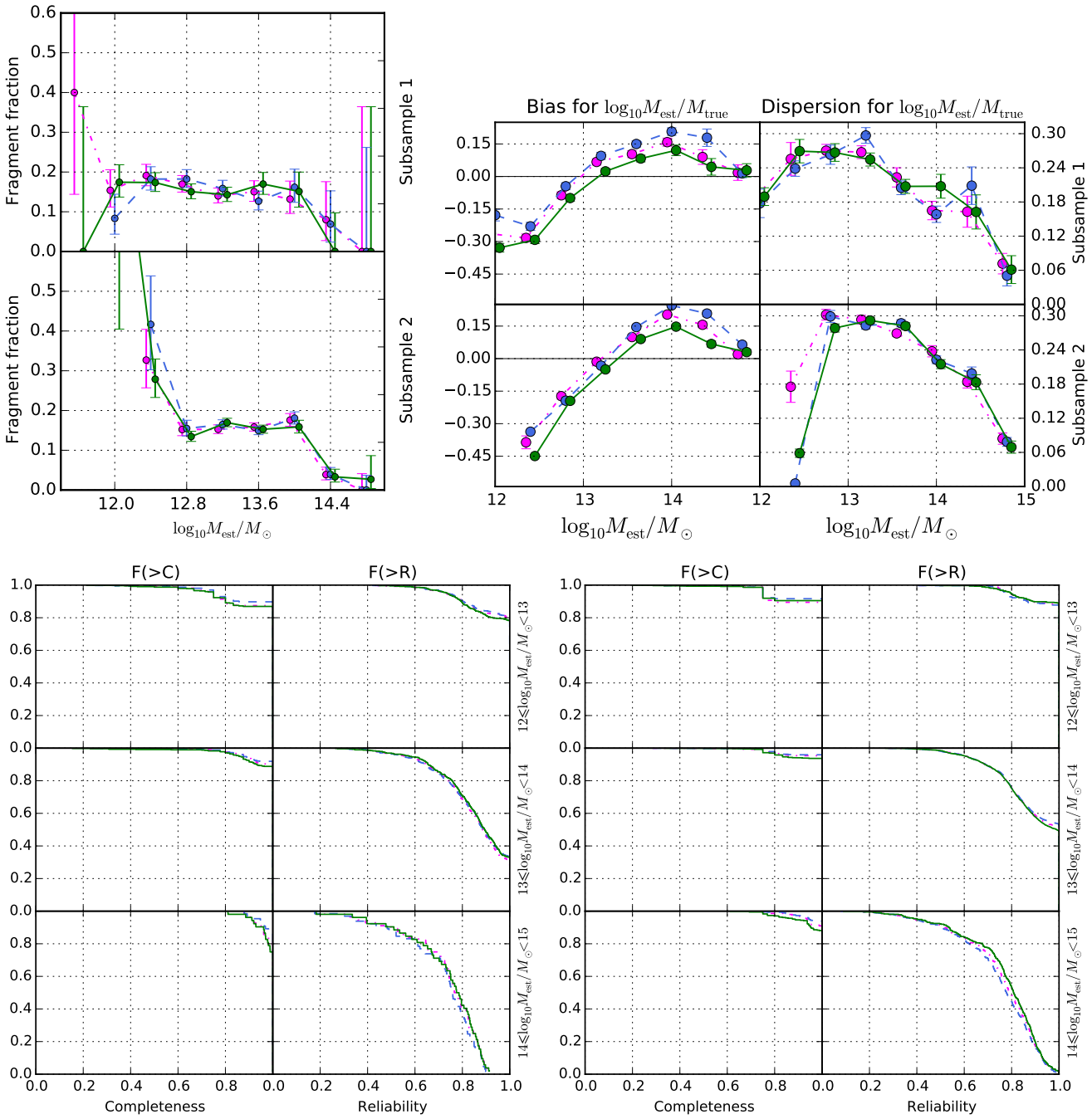

Figure 9. Effects of the choice of cosmological parameters on the fraction of fragments (*top left*), the accuracy in the recovered halo mass (*top right*), and the cumulative distribution functions of galaxy completeness and reliability of the groups (*bottom*) for MAGGIE-M (with 0.2 dex observational errors). The analysis is for unflagged groups of at least 3 true and 3 extracted members. The colour code is *green* for the Millennium Simulation cosmology ($\Omega_{\rm m}=0.25$, $h=0.73$), *magenta* for WMAP9 ($\Omega_{\rm m}=0.279$, $h=0.70$), and *royal blue* for Planck ($\Omega_{\rm m}=0.308$, $h=0.678$).

mock, lead to halo masses that are larger by the inverse ratio of Hubble constants in our AM technique.[15] This bias should thus be $\log(h_{\rm MS-II}/h_{\rm WMAP})\simeq 0.02$ and $\log(h_{\rm MS-II}/h_{\rm Planck})\simeq 0.03$, both independent of mass. The left panels of the upper right plots confirm that the bias is roughly independent of EG mass[16], but is roughly 3 times greater than expected.

This general lack of sensitivity to cosmological parameters is

[15] The group luminosities and stellar masses are also affected by the Hubble constant, but this does not affect the group total masses (halo masses) derived with AM, since the ranking of the group luminosities or stellar is independent of the Hubble constant, hence the first-rank group (by luminosity or stellar mass) will be assigned the highest halo mass, which scales as $1/h$, hence will be higher.

[16] We also find (not shown) that the bias in group total mass is even more independent of the true group mass.

expected, given the low maximal redshift of our subsamples ($z = 0.1$, see Table 1). One expects MAGGIE to be more sensitive to the choice of cosmological parameters when applied to deeper galaxy surveys.

5.3.4 *Effects of the form for the density of interlopers in projected phase space*

We now probe the sensitivity of MAGGIE-M to the choice of the functional forms that enter in the expression of the density of interlopers in PPS, $g_{\rm i}(R,v)$ (see eqs. [19] and [20]), namely the radial dependence of the normalization A and standard deviation $\sigma_{\rm i}$ of the Gaussian component of $g_{\rm i}$, as well as the level of the constant component, B.

Figure D1 in Appendix D shows only small effects (note that the symbols in the upper plots have their abscissa shifted for clarity) on the performance of MAGGIE-L and MAGGIE-M (both with observational errors) on group fragmentation, galaxy completeness and reliability and group mass accuracy, when switching from equations (21)-(23), derived by Mamon et al. (2010) on the dark matter particles of a hydrodynamical cosmological simulation to equations (24)-(26), that we fit to the mock that we extracted from the SAM by Guo et al. (2011).

5.4 Comparison of MAGGIE to other group finders

5.4.1 *Other grouping methods*

We now compare MAGGIE to other group finders. We first consider the FoF algorithm with the dimensionless linking lengths of $b_\perp = 0.06$ and $b_\parallel = 1.0$, which, in Paper I, we had determined to be optimal for studies of environmental effects on galaxies (for the cosmology of the mock we are using here). These linking lengths are close to the values $b_\perp = 0.06$, $b_\parallel = 1.08$ optimized by Robotham et al. (2011). We consider two implementations of the FoF, where, for testing purposes, the central galaxy is the most luminous ('FoF-L') or the most massive in stars ('FoF-M').

Yang et al. (2007) provided extensive tests of their group finder, but these are difficult to compare with ours, in particular, because 1) their mocks are flux-limited, so they had to include uncertain corrections for luminosity-incompleteness of groups in performing their AM, and 2) their mocks do not include observational errors. We therefore additionally consider a simple implementation of the Yang et al. (2005, 2007) group finder.

Yang et al. (2005, 2007) assigned a galaxy to a group according to a minimum density in PPS, which they transformed into a number density contrast of galaxies in redshift space:[17]

$$P_M(R,\Delta z) = \frac{H_0}{c}\,\frac{\Sigma_{\rm NFW}(R)}{\overline{n}}\,p_{\rm Gauss}(\Delta z|R) > \mathcal{B}\,, \qquad (33)$$

where $\overline{n}$ is the mean galaxy density at redshift $z_{\rm group}$, c is the speed of light, H_0 is the present-day Hubble constant, $\Sigma_{\rm NFW}(R)$ is the NFW surface density profile, $p_{\rm Gauss}$ is the Gaussian probability distribution function, $\Delta z = z - z_{\rm group}$, and $\mathcal{B}$ is the dimensionless local density contrast in redshift space.[18] Combining our notation with theirs, the total PPS density (what we would call $g = g_{\rm h} + g_{\rm i}$ in MAGGIE) is

$$\begin{aligned} g(R,v) &= \Sigma_{\rm NFW}(R)\,p_{\rm Gauss}(v|R) \\ &= \Sigma_{\rm NFW}(R)\left(\frac{1+z_{\rm group}}{c}\right)p_{\rm Gauss}(\Delta z|R) \qquad (34)\\ &= \frac{(1+z_{\rm group})}{H_0}\,\overline{n}\,P_M(R,\Delta z)\,, \qquad (35)\end{aligned}$$

where the second and third equalities are respectively obtained with equations (7) and (33). Equations (33) and (35) lead to an expression of the Yang et al. criterion in terms of the PPS density:

$$g(R,v) > \mathcal{B}\,\frac{(1+z_{\rm group})}{H_0}\,\overline{n}\,. \qquad (36)$$

In our implementation of the Yang et al. algorithm, the probabilities of membership of equation (8) are replaced by

$$p(R,v) = \begin{cases} 1 & \text{for } P_M(R,\Delta z) \geqslant \mathcal{B} \\ 0 & \text{for } P_M(R,\Delta z) < \mathcal{B}\,. \end{cases}\,, \qquad (37)$$

where equation (7) links v with Δz. In Appendix E, we argue that since we adopt different cosmological parameters (from the Millennium-II simulation) than Yang et al. did (from their cosmological simulations), we need to convert $\mathcal{B} = 10$ to $\mathcal{B} = 29$.[19] However, Figure E1 in Appendix E indicates that the fraction of EGs that adopting $\mathcal{B} = 10$ leads to slightly lower group fragmentation, much higher galaxy completeness, and less dispersed total masses than with $\mathcal{B} = 29$, but at the expense of much lower galaxy reliability. We therefore adopt $\mathcal{B} = 10$.

We have implemented the Yang et al. group finder in this fashion using AM to obtain halo masses with either the group luminosities (hereafter, Yang-L) or the group stellar masses (hereafter, Yang-M), which we collectively refer to as 'Yang'. Both of these implementations are a streamlined version of the Yang et al. (2005, 2007) group finder (which also has two flavours according the the observable used for the AM), as a full implementation is beyond the scope of the present article.

5.4.2 *Fragmentation*

Figure 10 shows that the fraction of FoF-L groups that are secondary fragments is over 30 percent for intermediate EG masses ($13 \leqslant \log M_{\rm est} \leqslant 14$), while the fraction of FoF-M groups that are secondary fragments is over 38 percent at all masses. In comparison, the fraction of MAGGIE and Yang et al. groups that are secondary fragments is typically less than 20%, on average nearly three times less than for FoF-M groups of the same estimated mass. This very high contamination of FoF groups by secondary fragments had already been noticed in Paper I, where the fraction of groups that are secondary fragments were found to be 49%, 23% and 46% for the 3 bins of estimated mass in the nearby subsample and 28%, 29% and 26% for the corresponding mass bins in the distant subsample. The higher fractions of FoF EGs that are secondary fragments found in the present work are caused by the inclusion of observational errors in our mock galaxy catalogue (in contrast to

[17] Equation (33) comes from writing the number of objects in a shell $(R, R+{\rm d}R)$ and redshift interval $(z, z+\Delta z)$ as $N(R,\Delta z) = 2\pi R\,\Sigma_{\rm NFW}(R)\,p_{\rm Gauss}(\Delta z|R)$, while the mean number of galaxies expected in the same volume $dV = 2\pi R\,{\rm d}R\,(c/H_0)\,{\rm d}\Delta z$ is $\overline{N} = \overline{n}\,{\rm d}V = 2\pi\,(c/H_0)\,\overline{n}\,R\,{\rm d}R\,{\rm d}\Delta z$.

[18] Yang et al. (2005, 2007) assume that $p_{\rm Gauss}(\Delta z|R)$ is in fact independent of R, i.e. that $\sigma_{\rm LOS}$ is independent of R.

[19] In Appendix E, we actually obtain $\mathcal{B} = 6.1$ for the cosmology adopted by Yang et al. (instead of $\mathcal{B} = 10$), which translates to $\mathcal{B} = 20$ in our cosmology.

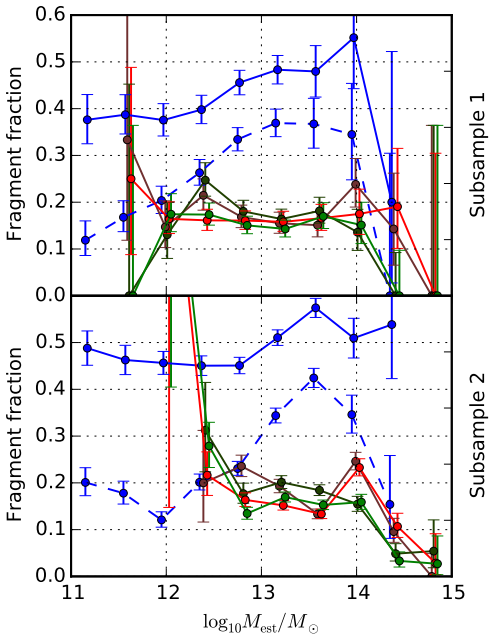

Figure 10. Fraction of extracted groups with MAGGIE-M, MAGGIE-L, FoF and our slimmed-down version of Yang et al. that are secondary fragments, as a function of their estimated group mass, for unflagged groups of at least 3 members (for both the extracted and true groups), for both the nearby (*top*) and distant (*bottom*) subsamples. The line colours are *green* for MAGGIE-M, *red* for MAGGIE-L, *blue* for FoF (with *dashed* and *solid lines* for FoF-L and FoF-M, respectively), *brown* for Yang-L and *dark green* for Yang-M (the latter two with threshold $\mathcal{B} = 10$). All group finders were run on a catalogue with errors of 0.2 dex on stellar masses. The error bars are computed with the Wilson (1927) formula. The points have their abscissa slightly shifted for clarity.

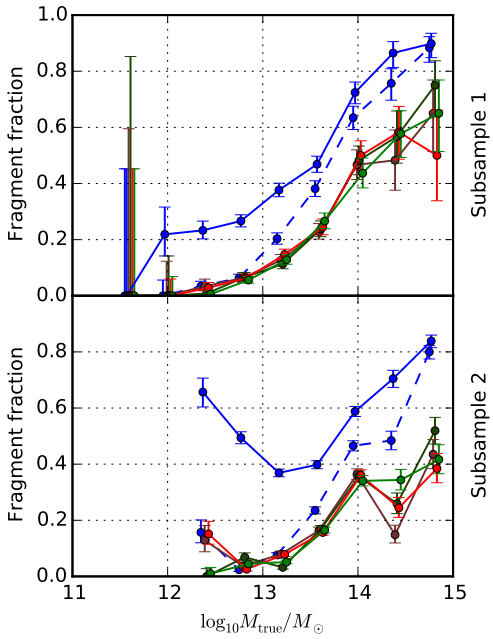

Figure 11. Same as Figure 10 but as a function of true group mass.

how we proceeded in Duarte & Mamon 2014), which sometimes substitutes the wrong galaxy for the central when matching the EG to the TG. This effect is more important for stellar masses than for luminosities, since the assumed observational errors are higher for the former (0.2 dex) than for the latter (0.08 dex).

The fraction of secondary fragments is quite similar between MAGGIE-L and Yang-L on one hand, and between MAGGIE-M and Yang-M on the other. On average, MAGGIE performs slightly better than Yang by a few percent in the absolute fraction of secondary fragments (4% and 2.5% for the L and M flavors, respectively), in the range $12.5 < \log M_{\rm est}/{\rm M}_\odot < 14$, which is statistically significant in the distant subsample (bottom panel of Fig. 10).

The fraction of secondary fragments in Figure 10 shows that the FoF EG masses are limited to $\log M_{\rm est}/{\rm M}_\odot = 14.4$. This is the consequence of the very high level of fragmentation at high TG masses, as illustrated in Figure 11. This high level of fragmentation of FoF groups at high TG mass was also seen in Figs. 4 and 6 of Paper I. While MAGGIE and Yang see their fraction of secondary fragments increase fairly moderately from 0 to 40 to 60 percent (depending on the subsample) from low to high TG masses, the FoF groups show much higher fractions of secondary fragments, increasing to over 80 percent at high TG masses.

In the lower portion [20] of the right panel of their figure 1,

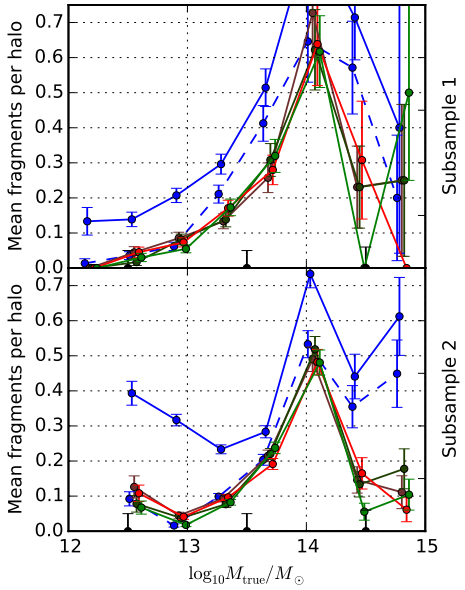

Figure 12. Mean number of secondary fragments (estimated mass between 0.1 and 1 times the true group mass) per true group as a function of true group mass for FoF (*blue*), MAGGIE-M (*green*), MAGGIE-L (*red*), our implementation of Yang et al. (*brown*, dashed and *solid* for $\mathcal{B} = 10$ and 29, respectively), and for Domínguez Romero et al. (2012, *black*). The *upper* and *lower* panels correspond to the nearby and distant subsamples, respectively, with the same Domínguez Romero et al. values in both. All catalogues were given errors of 0.2 dex in stellar mass, except MAGGIE-L, which performed AM with luminosities that were given 0.08 dex errors, and Domínguez Romero et al., which did not consider observational errors (and were measured on a flux-limited sample). The error bars indicate errors on means for all group finders except Domínguez Romero et al., for which standard deviations are used. The points have their abscissa slightly shifted for clarity.

[20] The two panels of figure 1 of Domínguez Romero et al. (2012) are confusing as they each mix two quantities.

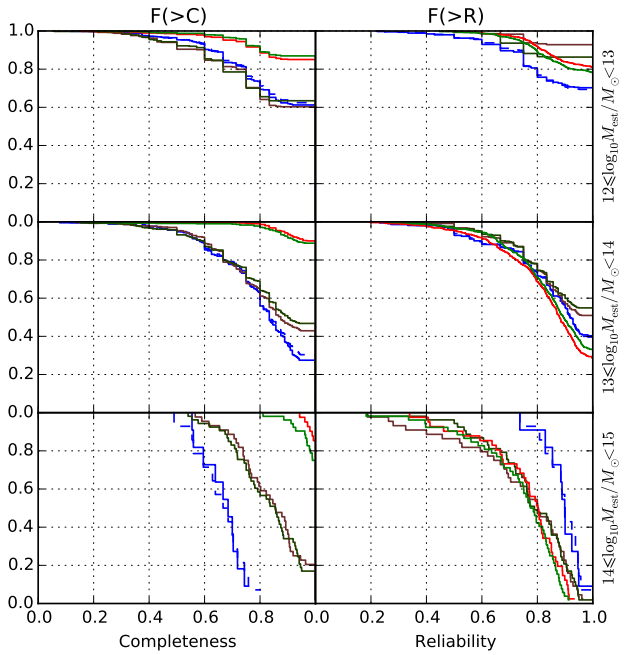

Figure 13. Cumulative distribution functions of the galaxy membership completeness (*left*, eq. [32]) and reliability (*right*, eq. [30]), for groups extracted with MAGGIE, FoF, and Yang for the nearby subsample (unflagged galaxies in groups of at least 3 members (for both the extracted and true groups) that are not secondary fragments . Both completeness and reliability are relative to the virial sphere of the true groups, and are derived in bins of estimated group masses. Same colours and line-types as in Fig. 10.

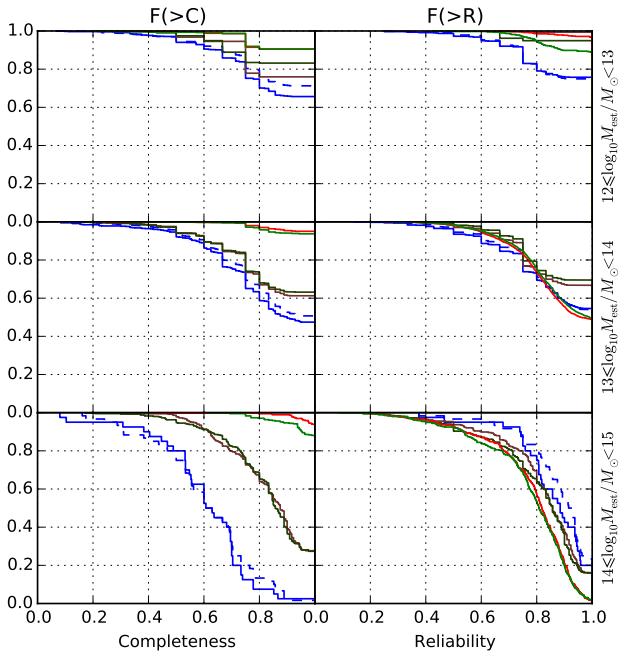

Figure 14. Same as Fig. 13, but for the distant sample. In the lowest mass bin, the completeness of MAGGIE-L is virtually the same as that of MAGGIE-M (which hides the former).

Domínguez Romero et al. (2012) found that the mean number of secondary fragments was zero with less than 0.05 errors at all TG masses. In contrast, MAGGIE and Yang lead to much higher mean numbers of fragments, while FoF is even worse.

However, Domínguez Romero et al. restricted their secondary fragments to those accounting for at least 10% of the TG mass, and defined their primary fragments as the most massive, while our definition of primary is the fragment containing the central galaxy.

Figure 15, further down, shows that a small minority of our secondary fragments are more massive than the TG, so to make a clean comparison with Domínguez Romero et al., we show in Figure 12 the mean number of secondary fragments with mass between one-tenth and one times the TG mass. Fragmentation worsens with increasing TG mass, as we had found in Paper I for FoF. But Figure 12 also indicates that, using the measure of group fragmentation of Domínguez Romero et al., MAGGIE, Yang and FoF are unable to match the zero mean number of secondary fragments per TG that Domínguez Romero et al. found. This discrepancy would be even stronger had we used errors on the means instead of standard deviations for the points of Domínguez Romero et al..

5.4.3 Galaxy completeness

The left panels of Figures 13 and 14 show that the galaxy completeness of MAGGIE is considerably higher than for FoF and Yang, regardless of the flavour (L or M). For example, according to Figure 14, the fractions of EGs in the distant subsample (which has better statistics) with better than 80 percent incompleteness are 91, 97 and 97 percent for MAGGIE-M and even higher for MAGGIE-L, compared to 80, 73 and 67 percent for Yang and 77, 63 and only 9 percent for FoF. Similar values are found for the nearby subsample (Fig. 13). The superior galaxy completeness of MAGGIE relative to Yang is statistically significant (with the KS test) in all three EG mass bins and in both subsamples. Similarly, Yang is significantly more complete than FoF in all EG mass bins and in both subsamples, except for the low EG mass bin of the nearby subsample, for which FoF is significantly more complete than Yang.

The decrease of galaxy completeness with increasing group mass was already noticed by Yang et al. (2007) (upper panels of their figure 2), although this decrease in completeness with mass is not as severe in their study, which considers bins of TG mass rather than EG mass (and is also for a flux-limited sample).

The left panel of figure 2 of Domínguez Romero et al. indicates median galaxy completeness of 96%, 91% and 92% for the three mass bins we used here (but for TG masses). In contrast, according to Figures 13 and 14, we arrive at median galaxy completeness of 100 percent for MAGGIE in all mass bins and in both subsamples, while our implementation of the Yang algorithm leads to 100 percent galaxy completeness in the low mass bin, 85 percent in the high mass bin (somewhat worse in bins of true mass). A more direct test involves a comparison to the flux-limited mock analyzed by Yang et al. (2007), whose upper left panel of figure 2 indicates 100 percent completeness in all mass bins.

The FoF algorithm produces increasingly incomplete galaxy extractions for increasing estimated group masses (see above). The lower galaxy completeness of FoF at high estimated group masses is a consequence of the very high fragmentation of high mass real-space groups (see Fig. 11). If a TG has non-negligible secondary fragments, then its primary fragment will tend to be incomplete. Consider, for example, a TG with 5 galaxies that is fragmented into an EG of 3 galaxies (containing the TG's central) and another EG of 2 galaxies; the EG of 3 galaxies will have a completeness of 3/5=0.6, a reliability of unity, and will not be counted as a secondary fragment, while the EG of 2 galaxies will be considered a

secondary fragment, but will not have completeness and reliability measured.

Finally, we compare the completeness levels to those that Muñoz-Cuartas & Müller (2012) derived from the analysis of the groups of at least two members that they extracted with their FoF-like group finder on a doubly complete subsample with $M_r < -19$ (matching our nearby doubly complete subsample). According to the bottom panel of their figure 13, the fraction of their EGs with over 90% completeness is 82%. In contrast, in the nearby subsample, our Figure 2 indicates that the fractions of EGs with 90% galaxy completeness are higher in all mass bins: 85%, 94%, and 100% for MAGGIE-L and 87%, 92%, and 96% for MAGGIE-M.

5.4.4 *Galaxy reliability*

The right hand panels of Figures 13 and 14 indicate that the rankings of the group finders in terms of galaxy reliability depend on EG mass. For the distant subsample (which has better statistics), at low EG mass (upper right panel of Fig. 14), the fraction of groups with 100 percent reliability is higher with Yang (90 percent) than with MAGGIE (80 percent) or FoF (70 percent). At 80 percent reliability, MAGGIE and Yang have similar reliabilities (90 percent). The overall differences in the CDFs, as quantified by the KS test, indicate that overall, Yang-M is significantly more reliable than MAGGIE-M, while Yang-L and MAGGIE-L cannot be distinguished. In turn, MAGGIE is significantly more reliable than FoF.

At intermediate EG mass (middle right panel of Fig. 14), all three group finders lead to similar fractions of roughly three-quarters of groups with over 80 percent reliability (80 percent for Yang-M). Yang is significantly more reliable than either MAGGIE or FoF, while MAGGIE is signficantly more reliable than FoF (although FoF has a marginally significantly higher fraction of groups with 100 percent reliability).

At high EG mass (lower right panel of Fig. 14), there is a clear hierarchy, where FoF is significantly more reliable than Yang, which in turn is significantly more reliable than MAGGIE. The fraction of groups with 80 percent reliability is roughly 80 percent for FoF, roughly two-thirds for Yang and slightly more than half for MAGGIE.

Our probabilistic method of measuring MAGGIE's galaxy reliability (eq. [30]) leads to values that are rarely low or near 100 percent. This can be clearly seen in the intermediate-mass EG groups (middle right panel of Fig. 14), where for MAGGIE relative to FoF or Yang, the decrease of the CDF is slower for reliabilities below 80 percent and faster at higher reliabilities.

5.4.5 *Mass accuracy*

Figure 15 shows how the estimated total masses (of the EGs) compare with the total masses (within the virial sphere) of the TGs (for clarity, we hereafter drop the term 'total' before 'mass' in this subsection), both for the primary (large coloured circles) and secondary (black crosses) fragments.

The FoF method, with the virial theorem to estimate masses (with the formula from Heisler et al. 1985), leads to frequent strong underestimation of the mass for the primary fragments of low-mass TGs. This is analogous to what is found by most group mass estimation methods when the group center and its velocity are provided (see Old et al. 2014, although Old et al. 2015 find that a Bayesian fitted slope of the estimated versus true mass relation is typically unity). Figure 15 shows that MAGGIE and Yang do not underestimate the EG masses of primary fragments as frequently as does the

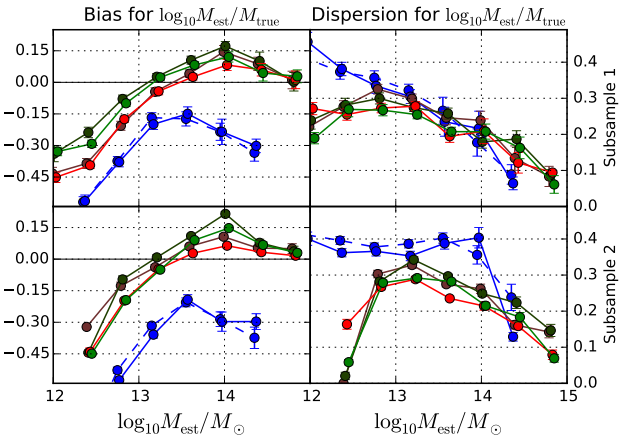

Figure 16. Median bias and scatter (using 16th and 84th percentiles) of extracted group total mass within the virial sphere, for groups extracted with MAGGIE, FoF, and our implementation of Yang et al.. The *top* and *bottom* panels are for nearby and distant subsamples, respectively (for unflagged primary groups of at least 3 true and 3 extracted members), The error bars for the bias and scatter are respectively $\sigma/\sqrt{N}$ and $\sigma/2\,[2/(N-1)+\kappa/N]^{1/2}$, where κ is the kurtosis excess. Same colours as Figure 10.

FoF algorithm. This better behaviour is likely to be the result of the use of AM to derive group masses.

As expected, in secondary fragments, the estimated mass is usually lower than the TG mass (often by several dex). However, in some secondary fragments, the estimated mass is higher than the TG mass. This can occur when the group luminosity or stellar mass is higher in the group with the lower central luminosity or stellar mass (which is how secondary fragments are defined). Figure 15 also shows that the trend of estimated versus true mass for the secondary fragments has a shallower slope than unity in contrast with the analogous trend for primary fragments.

The left panels of Figures 15 and 16 show that the virial-theorem masses of FoF EGs are biased low by a factor as great as 10 at the lowest estimated masses and by over 0.15 dex at high estimated masses. Similar trends of strong mass underestimation with FoF were found in Paper I for low-richness EGs. The mass biases of MAGGIE and Yang vary in a similar way as a function of EG mass as for FoF, except that the biases are much lower (the mass ratio is much closer to unity): while the FoF mass bias is greater than 15% at all EG masses, the mass biases of MAGGIE and Yang are better than 15% for $\log M_{\rm est}/{\rm M}_\odot > 13$.

Since bias can, in principle, be corrected for, it is more important to consider the scatter in the mass estimation. The right hand panels of Figure 16 indicate that, at low EG masses, FoF EGs have much greater mass dispersion than their MAGGIE and Yang counterparts. For example, at $\log M_{\rm est}/{\rm M}_\odot \simeq 12.7$, the FoF mass scatter is 0.1 dex worse than that of MAGGIE, with Yang in between (nearby subsample) or as good as MAGGIE (distant subsample).

At intermediate EG masses, MAGGIE remains the group finder with the lowest scatter in group masses (roughly 0.24 and 0.26 dex in the nearby and distant subsamples, respectively), with Yang slightly worse (0.25 dex and 0.30 dex scatter respectively), and FoF slightly worse than Yang in the nearby subsample (0.28 dex scatter) and much worse in the distant subsample (0.38 dex scatter). Given the errors in the dispersions, these trends are statistically significant.

At high EG masses, the hierarchy between group finders is

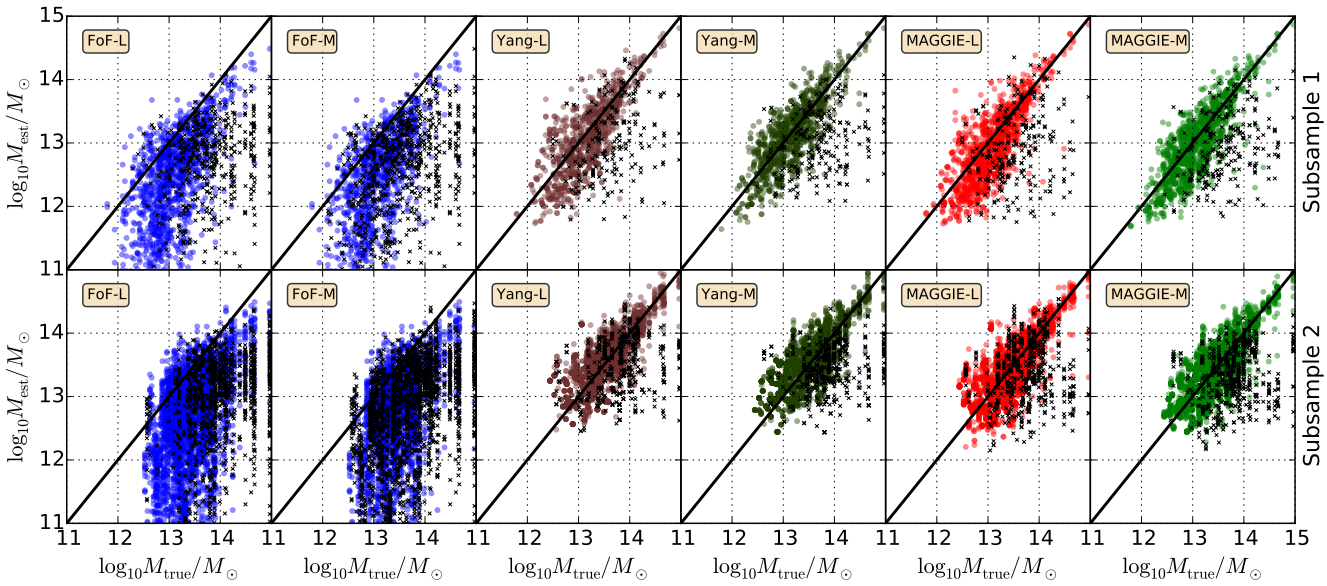

Figure 15. Estimated mass versus true mass for the unflagged non-secondary (*filled coloured circles*) and secondary (*black crosses*) EGs with at least 3 members (for both the extracted and true groups) for six group finders (from left to right): FoF-L, FoF-M, Yang-L, Yang-M (both with $\mathcal{B} = 10$), MAGGIE-L, and MAGGIE-M. The *diagonal lines* indicate perfect mass recovery. There are roughly as many MAGGIE groups as there are FoF groups, but the former occupy identical positions in the plots due to the replications of the simulation boxes causing identical stellar masses, hence identical group masses after the AM used to infer group masses.

more difficult to appraise. The factor of 2 typical underestimate of group masses with FoF prevents high EG masses with FoF, which explains why no points for FoF beyond $\log M_{\rm est}/{\rm M}_\odot = 14.4$ in Figure 16. At this EG mass, FoF-M produces lower dispersion (0.06 and 0.12 dex for the nearby and distant subsamples, respectively), while FoF-L is not as accurate (0.09 and 0.24 for the two subsamples, respectively). At this EG mass, the corresponding dispersions on EG masses are 0.12, 0.13, 0.17 and 0.19 for MAGGIE-L, Yang-L, MAGGIE-M and Yang-M for the nearby subsample, and 0.16, 0.16, 0.18 and 0.22 for the distant subsample (in the same order of group finders). Averaged over the full bin of high EG masses, while MAGGIE and Yang are comparable in the nearby subsample, while MAGGIE is more accurate than Yang by 0.04 dex in the distant subsample.

The scatter in group total mass of the original Yang et al. algorithm was shown in figure 7 of Yang et al. (2007). Considering the case where no correction for luminosity incompleteness is required (their panel c), one finds that the scatter divided by $\sqrt{2}$ is $\sigma_Q \approx 0.23$ for group estimated log masses in the range 12 to 14.4 (solar units), leading to a scatter of $\sqrt{2}\times0.23$=0.33.[21]

The dispersion in group mass found with our implementation of Yang on our doubly-complete subsamples (with observational errors) are thus much lower, and diminish with increasing EG mass from 0.3 dex to 0.1 dex (right panels of Fig. 16), contrary to the situation with the flux-limited sample (without observational errors) analyzed by Yang et al. (2007).

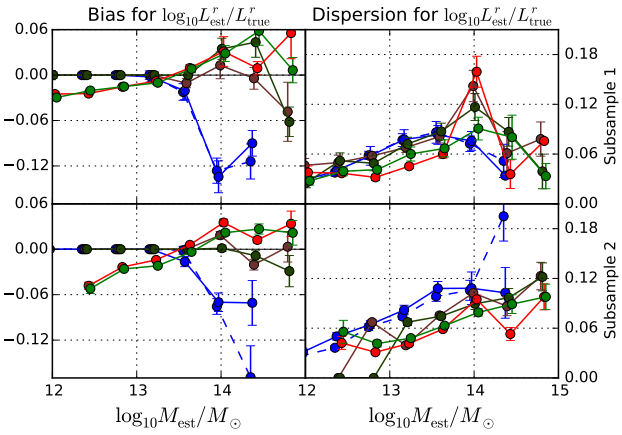

Figure 17. Median bias and scatter (using 16th and 84th percentiles) of extracted group luminosity within the virial sphere, for groups extracted with MAGGIE, FoF, and our implementation of Yang et al.. The *top* and *bottom* panels are for nearby and distant subsamples, respectively (for unflagged primary groups of at least 3 true and 3 extracted members), The error bars for the bias and scatter are respectively $\sigma/\sqrt{N}$ and $\sigma/2\,[2/(N-1)+\kappa/N]^{1/2}$, where κ is the kurtosis excess. Same colours as Figure 10.

5.4.6 *Accuracy of group luminosity and stellar mass*

Figures 17 and 18 respectively show the accuracy on EG luminosities and stellar masses. The left panels of both figures show that, at low EG mass, FoF and Yang have zero median bias of lumi-

[21] We do not understand the factor of $\sqrt{2}$ in eq. (14) of Yang et al. (2007), since the halo masses to which the group masses are compared are highly accurate as they are derived by summing over 1000 simulation particles, leading to 0.014 dex mass scatter from Poisson shot noise.

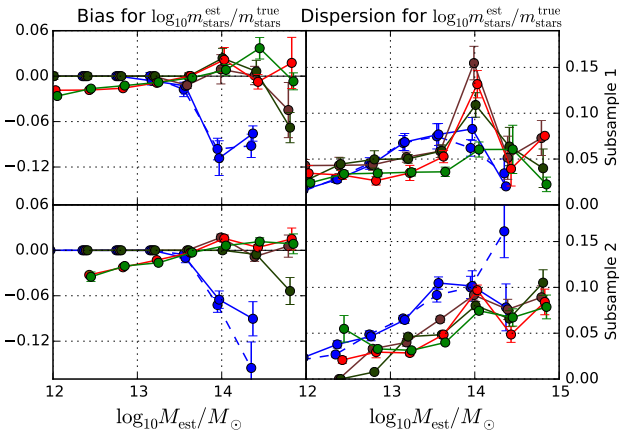
Bias for $\log_{10} m^{\rm est}_{\rm stars}/m^{\rm true}_{\rm stars}$
Dispersion for $\log_{10} m^{\rm est}_{\rm stars}/m^{\rm true}_{\rm stars}$
Subsample 1
Subsample 2
$\log_{10} M_{\rm est}/M_\odot$
$\log_{10} M_{\rm est}/M_\odot$

Figure 18. Median bias and scatter (using 16th and 84th percentiles) of extracted group stellar mass within the virial sphere, for groups extracted with MAGGIE, FoF, and our implementation of Yang et al.. The *top* and *bottom* panels are for nearby and distant subsamples, respectively (for unflagged primary groups of at least 3 true and 3 extracted members), The error bars for the bias and scatter are respectively $\sigma/\sqrt{N}$ and $\sigma/2\,[2/(N-1)+\kappa/N]^{1/2}$, where κ is the kurtosis excess. Same colours as Figure 10.

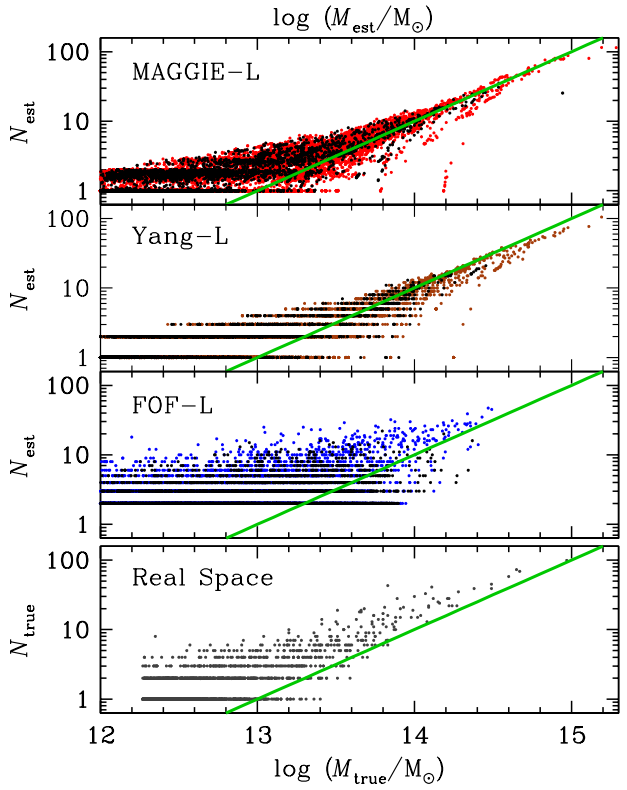

Figure 19. Group richness versus total mass. *Top three panels*: Estimated quantities for unflagged groups extracted with MAGGIE-L (*top*), Yang-L (*middle*), and FoF-L (*bottom*), all for the distant subsample. The primary fragments are shown in colour (*red* for MAGGIE-L, *brown* for Yang-L, and *blue* for FoF-L), while the secondary fragments are shown in *black*. *Bottom panel*: True richness (galaxies more luminous than $M_r = -20.5$, which corresponds to the luminosity limit of the distant subsample) versus total mass of real space groups (*dark grey*). In all panels, the *thick green line* shows $N = M/10^{13}{\rm M}_\odot$, simply to guide the eye.

nosity and stellar mass, while MAGGIE is biased low (always less than 0.05 dex). The median bias of zero for FoF and Yang is expected since the reliability of the primary EGs in the low EG mass bin is 100 percent for all group finders. The negative median bias of MAGGIE at low EG mass must therefore be linked to its probabilistic method of measuring luminosity (eq. [27]) and stellar mass (eq. [28]).

At intermediate EG mass, the biases in luminosity and stellar mass with Yang-M remain at zero, those with Yang-L are within 0.01 dex of zero, those with MAGGIE increase to typically 0.03 dex from zero, while those with FoF decrease to reach –0.07 (–0.12) dex at $\log M_{\rm est}/{\rm M}_\odot = 14.0$ for the distant (nearby) subsample.

At high EG mass, Yang and MAGGIE have comparable biases in luminosity and stellar mass, typically within 0.03 dex from zero (except Yang-M at the highest EG mass bin for stellar masses, which is biased low by typically 0.06 dex). On the other hand, the group luminosities and stellar masses are biased low by FoF by typically –0.08 dex for FoF-M and as much or worse than –0.10 dex for FoF-L (all with fairly large uncertainties).

The FoF, Yang and MAGGIE group finders all lead to comparable inefficiencies in EG luminosity or stellar mass in the low EG mass bin of the nearby subsample, 0.04 dex for MAGGIE and 0.045 dex for FoF, and 0.05 dex for Yang. In the distant subsample, while FoF remains at 0.05 (luminosities) or 0.04 (stellar masses) dex inefficiency, MAGGIE has lower dispersion of 0.03 dex, while Yang reaches even lower dispersions at the lowest EG masses.

At intermediate EG mass, EGs extracted with FoF have the highest dispersion (typically 0.09 dex), while MAGGIE EGs have the lowest dispersion in luminosity and stellar mass (typically 0.05 dex), and Yang EGs are in between. However, MAGGIE-L and Yang-L (to a lesser extent) have a spike in dispersion in luminosity and stellar mass at $\log M_{\rm est}/{\rm M}_\odot = 14.0$ in the nearby subsample.

At high EG masses ($\log M_{\rm est}/{\rm M}_\odot > 14.0$), FoF groups only reach $\log M_{\rm est}/{\rm M}_\odot > 14.4$. At that EG mass, FoF and MAGGIE-L groups have the lowest dispersions in luminosity and stellar mass in the nearby subsample (typically 0.04 dex only), whereas MAGGIE-M and Yang-M have the highest dispersions (0.06 dex in luminosity and 0.08 dex in stellar mass), while Yang-L is in between. In the distant subsample at the same EG mass, all group finders lead to the same dispersions in luminosity (0.09 dex) and stellar mass (0.075 dex), except that MAGGIE-L has significantly lower dispersions (0.05 dex), while FoF-L has very high dispersions (over 0.16 dex). At the highest EG mass, where $\log M_{\rm est}/{\rm M}_\odot = 14.8$, MAGGIE-M and Yang-M lead to the lowest dispersions in the nearby subsample (0.03 dex only), while MAGGIE-L and Yang-L are marginally less efficient (0.075 dex). In the distant subsample at this very high EG mass, both flavours of MAGGIE lead to the lowest dispersions in luminosity and stellar mass (0.10 dex in luminosity and 0.08 dex in stellar mass), while Yang-M is marginally worse (0.12 dex in luminosity and 0.10 dex in stellar mass).

5.4.7 *Richnesss versus total mass*

We complete the comparison of MAGGIE with Yang and FoF by comparing the richness - mass relations of the three group finders. Figure 19 shows the estimated richness versus the estimate mass for MAGGIE-L, Yang-L and FoF-L, as well as the true richness versus true mass (where the richness is measured for galaxies more luminous than $M_r = -20.5$, conforming to the luminosity limit of the

distant subsample).[22] The richness-mass relations of MAGGIE and Yang resemble one another, although the estimated galaxy numbers are integers for Yang (and FoF), while they are floating numbers for MAGGIE, making the figure for MAGGIE more continuous. In particular the mean trend and scatter are very similar. On the other hand, the poor mass accuracy of FoF causes scatter and the negative bias of mass shows here as higher richness for given mass. The richness mass relations are very similar for the nearby sample and for the M flavour of the three group finders. One also notices in Figure 19 that the overall trend of the estimated richness-mass relations match fairly well that of the true relation, with Yang, and to a lesser extend MAGGIE showing slight negative bias in richness at given mass relative to the real-space trend.

5.4.8 Synthesis

A comparison of MAGGIE with other group finders, performed on the same mock catalogue, with the same observational errors, does not point to a single superior group finder among the 6 tested group finders (3 algorithms: MAGGIE, FoF and Yang; 2 definitions of central galaxy: most luminous or most massive in stars).

Since most of our tests involve the primary fragments of the EGs, group fragmentation appears to be the most serious issue. Our tests indicate that MAGGIE has the least group fragmentation, with Yang a close second, while FoF suffers tremendously from group fragmentation. This hierarchy is repeated when we consider galaxy completeness of primary groups, which is related to group fragmentation, since groups with important secondary fragments will necessarily have lower galaxy completeness.

Galaxy reliability is generally the highest in the Yang group finder, with MAGGIE second and FoF last, except at high EG masses, where FoF is most reliable while MAGGIE is the least.

Group total mass is severely underestimated by the virial theorem mass of the FoF group finder. This, again, is a consequence of the heavy fragmentation of FoF groups. MAGGIE and Yang perform much better, with a slight advantage for MAGGIE. The ranking of the group finders concerning the dispersion in group total mass depends on the interval of EG mass considered. At low EG mass, FoF performs poorly and Yang performs slightly better than MAGGIE. At intermediate EG mass, MAGGIE performs slightly better than Yang (starting at $\log M_{\rm est}/{\rm M}_\odot = 12.5$) and considerably better than FoF. At high EG mass, MAGGIE performs slightly better than Yang, with FoF even better, but limited to half the high EG mass bin, given its negative bias.

Group luminosity and stellar mass are measured without bias with FoF and Yang for low EG mass groups, while MAGGIE is slightly biased low (by typically less than 0.05 dex). At intermediate EG mass, Yang EG luminosities and stellar masses remain unbiased, FoF is biased low and MAGGIE is only slightly biased (in either direction). At high EG mass, MAGGIE is the least biased and FoF the most.

Finally, the richness-mass relations of MAGGIE and Yang are much less scattered than that of FoF, although MAGGIE and Yang are biased low in richness (at given mass), by 0.2 dex (MAGGIE) and 0.3 dex (Yang), while FoF is not.

In summary, relative to FoF, MAGGIE suffers much less from fragmentation, is much more complete, more reliable, except at high EG masses, with much less biased group masses, considerably less dispersed group masses, except for cluster-mass EGs, and produces more accurate group luminosities and stellar masses, except for low-mass EGs, where the median bias although very small, is not zero as in FoF.

Relative to our implementation of Yang, MAGGIE is slightly less affected by group fragmentation, considerably more complete but less reliable in its galaxy membership, slightly more accurate in group total masses, slightly more biased but slightly less dispersed in group luminosities and stellar masses.

These tests permit to assess how the characteristics of the group finder influence its performance in reproducing the real space groups. FoF is a group finder that makes no assumptions on the physics of groups and of projection effects (once its linking lengths have been optimized). The group finder by Yang et al. (2005, 2007) introduced priors on the galaxy distribution in PPS as well as abundance matching to determine EG masses. MAGGIE improved the adopted priors on the distribution of galaxies in PPS and adopted a probabilistic approach for the membership of galaxies in groups, following Domínguez Romero et al. (2012), but keeping the memberships probabilistic instead of finishing with hard group assignments as done by Domínguez Romero et al.. Our tests indicate that, overall, there are fewer differences between MAGGIE and Yang, than between either and FoF. This suggests that the probabilistic membership of MAGGIE and its more refined priors on the distribution of galaxies in PPS play a smaller role than the use of priors, as well as the AM used for measuring group masses.

6 CONCLUSIONS

We have introduced a new prior, halo-based and fully probabilistic group finder called MAGGIE, where the total group/cluster masses are obtained by abundance matching between the assumed known halo mass function and the derived group luminosity (MAGGIE-L) or stellar mass (MAGGIE-M) function. This grouping algorithm is similar to that of Yang et al. (2005, 2007), but uses a more refined and probabilistic membership criterion, and is meant to be applied to subsamples that are complete in both luminosity and distance, to avoid the unavoidable luminosity incompleteness in flux limited samples, which are very difficult to accurately correct for.

We extensively tested MAGGIE as well as our implementations of the FoF group finder with the optimal linking lengths derived by Duarte & Mamon (2014) as well as a simplified version of the group finder of Yang et al. (2005, 2007). For our tests, we used a mock SDSS Legacy spectroscopic survey derived from the Guo et al. (2011) SAM, itself run on the Millennium-II cosmological dark matter simulation. We also compared the performances of MAGGIE with the similar published tests by Yang et al. (2007) and Domínguez Romero et al. (2012) and Muñoz-Cuartas & Müller (2012) of their respective group finders, in all instances where this could be done.

We find that both flavours of MAGGIE perform better than FoF in all our tests (fragmentation, galaxy completeness and reliability, accuracy in group total mass, luminosity and stellar mass), except for cluster-mass EGs, where MAGGIE produces less reliable galaxy members and more dispersed total masses. The superiority of MAGGIE relative to FoF appears to be linked with the very high fraction of secondary fragments that FoF produces.

The performance of MAGGIE is much closer to that of our simple implementation of the Yang et al. group finder: MAGGIE performs much better on galaxy completeness, slightly better on group

[22] The lower number of groups in the Real Space panel is a consequence of the smaller volume of the Millennium-II simulation box in comparison to that of the distant doubly complete subsample.

fragmentation, and dispersion of group total masses, luminosities and stellar masses, but slightly worse on bias in group luminosities and stellar masses, and also worse on galaxy reliabilities.

Given its use of realistic priors, abundance matching and probabilistic galaxy membership, MAGGIE-M is an ideal grouping algorithm to be applied on large galaxy spectroscopic surveys such as the Sloan Digital Sky Survey (SDSS) and the Galaxy And Mass Assembly (GAMA), for several applications: environmental effects on galaxy properties such as SSFR, as well as mass/orbit modelling of groups and clusters (possibly stacking the groups), for which MAGGIE will lead to more realistic results compared to the Yang et al. group finder, given the more realstic prirors of the former. Moreover, MAGGIE should in principle be able to work for much deeper spectroscopic surveys, possibly including surveys based upon photometric redshifts (since MAGGIE naturally handles redshift errors), with applications to the evolution of environmental effects, dark matter properties (normalization, concentration), and velocity anisotropy (orbital shapes).

In particular, MAGGIE should be very useful for dark energy surveys such as the Dark Energy Survey (DES), Euclid, and the Wide-Field Infrared Survey Telescope (WFIRST, yet to be approved) that will constrain dark energy parameters not only with cosmic shear and baryonic acoustic oscillations, but also by measuring the mass function and clustering of galaxy clusters. However, the abundance matching method – used to determine group masses – involves an assumption on the halo mass function, which is cosmology-dependent. This implies that the current implementation of MAGGIE cannot be used as a cosmographic tool to determine cosmological parameters from the derived halo mass function. Nevertheless, MAGGIE should be an excellent tool to optimally detect and measure groups and clusters in dark energy surveys, if a given cosmology is assumed. Moreover, by replacing abundance matching by other techniques, MAGGIE could be adapted into a powerful cosmographic tool for such surveys.

ACKNOWLEDGMENTS

Paper I and this article were part of the doctoral thesis of MD. We thank Radek Wojtak for encouraging us to avoid hard assignments of galaxies to their final groups in our probabilistic group finder, at a time when we were still hesitant on the approach. We also warmly thank Reinaldo de Carvalho for a thorough reading of an earlier draft with constructive criticisms, Xiaohu Yang and Mariano Domínguez Romero for explaining details of their respective group finders, as well as David Valls-Gabaud, Andrea Biviano, Begoña Ascaso and Florence Durret for useful comments. We finally thank the anonymous referee for his/her insightful and constructive comments that significantly improved this work. The Millennium-II Simulation database used in this paper and the web application providing online access to them were constructed as part of the activities of the German Astrophysical Virtual Observatory (GAVO). We are grateful to Michael Boylan-Kolchin and Qi Guo for respectively allowing the outputs of the Millennium-II simulation and the Guo semi-analytical model to be available to the public, and Gerard Lemson for maintaining the GAVO database and for useful discussions. We also made use of HMFCALC (Murray et al. 2013) to check our computations of halo mass functions.

REFERENCES

Abazajian K. N. et al., 2009, ApJS, 182, 543
Abell G. O., 1958, ApJS, 3, 211
Ascaso B., Wittman D., Benítez N., 2012, MNRAS, 420, 1167
Beers T. C., Tonry J. L., 1986, ApJ, 300, 557
Behroozi P. S., Conroy C., Wechsler R. H., 2010, ApJ, 717, 379
Bennett C. L. et al., 2013, ApJS, 208, 20
Beraldo e Silva L., Mamon G. A., Duarte M., Wojtak R., Peirani S., Boué G., 2015, MNRAS, 452, 944
Berlind A. A. et al., 2006, ApJS, 167, 1
Blaizot J., Wadadekar Y., Guiderdoni B., Colombi S. T., Bertin E., Bouchet F. R., Devriendt J. E. G., Hatton S., 2005, MNRAS, 360, 159
Borgani S. et al., 2004, MNRAS, 348, 1078
Boylan-Kolchin M., Springel V., White S. D. M., Jenkins A., Lemson G., 2009, MNRAS, 398, 1150
Brinchmann J., Charlot S., Heckman T. M., Kauffmann G., Tremonti C., White S. D. M., 2004, ArXiv Astrophysics e-prints, arXiv:astro-ph/0406220
Bruzual G., Charlot S., 2003, MNRAS, 344, 1000
Cattaneo A., Mamon G. A., Warnick K., Knebe A., 2011, A&A, 533, A5
Chen Y.-M. et al., 2012, MNRAS, 421, 314
Chilingarian I. V., Melchior A.-L., Zolotukhin I. Y., 2010, MNRAS, 405, 1409
Cole S., Lacey C., 1996, MNRAS, 281, 716
Colless M. et al., 2001, MNRAS, 328, 1039
Conroy C., Gunn J. E., White M., 2009, ApJ, 699, 486
Courtin J., Rasera Y., Alimi J.-M., Corasaniti P.-S., Boucher V., Füzfa A., 2011, MNRAS, 410, 1911
Crocce M., Fosalba P., Castander F. J., Gaztañaga E., 2010, MNRAS, 403, 1353
Domínguez Romero M. J. d. L., García Lambas D., Muriel H., 2012, MNRAS, 427, L6
Duarte M., Mamon G. A., 2014, MNRAS, 440, 1763, paper I
Eisenstein D. J., 1997, ArXiv Astrophysics e-prints, arXiv:astro-ph/9709054
Eke V. R. et al., 2004, MNRAS, 348, 866
Falco M., Mamon G. A., Wojtak R., Hansen S. H., Gottlöber S., 2013, MNRAS, 436, 2639
Gerke B. F. et al., 2005, ApJ, 625, 6
Gladders M. D., Yee H. K. C., 2000, AJ, 120, 2148
Gunn J. E., Gott J. R., 1972, ApJ, 176, 1
Guo Q. et al., 2011, MNRAS, 413, 101
Heisler J., Tremaine S., Bahcall J. N., 1985, ApJ, 298, 8
Hickson P., 1982, ApJ, 255, 382
Hopkins A. M. et al., 2013, MNRAS, 430, 2047
Hubble E. P., 1936, Realm of the Nebulae. Yale University Press, New Haven
Huchra J. P., Geller M. J., 1982, ApJ, 257, 423
Jackson J. C., 1972, MNRAS, 156, 1P
Jenkins A., Frenk C. S., White S. D. M., Colberg J. M., Cole S., Evrard A. E., Couchman H. M. P., Yoshida N., 2001, MNRAS, 321, 372
Jones D. H. et al., 2009, MNRAS, 399, 683
Kennicutt, Jr. R. C., Bothun G. D., Schommer R. A., 1984, AJ, 89, 1279
Larson R. B., Tinsley B. M., Caldwell C. N., 1980, ApJ, 237, 692
Liu D.-Z., Ma C., Zhang T.-J., Yang Z., 2011, MNRAS, 412, 2685
Liu H. B., Hsieh B. C., Ho P. T. P., Lin L., Yan R., 2008, ApJ, 681, 1046

Macciò A. V., Dutton A. A., van den Bosch F. C., 2008, MNRAS, 391, 1940
Mamon G. A., 1992, ApJ, 401, L3
Mamon G. A., Biviano A., Boué G., 2013, MNRAS, 429, 3079
Mamon G. A., Biviano A., Murante G., 2010, A&A, 520, A30
Mamon G. A., Łokas E. L., 2005, MNRAS, 363, 705
Maraston C., Strömbäck G., 2011, MNRAS, 418, 2785
Maraston C., Strömbäck G., Thomas D., Wake D. A., Nichol R. C., 2009, MNRAS, 394, L107
Marinoni C., Davis M., Newman J. A., Coil A. L., 2002, ApJ, 580, 122
Marinoni C., Hudson M. J., 2002, ApJ, 569, 101
Mendel J. T., Simard L., Palmer M., Ellison S. L., Patton D. R., 2014, ApJS, 210, 3
Merritt D., 1987, ApJ, 313, 121
Muñoz-Cuartas J. C., Müller V., 2012, MNRAS, 423, 1583
Murray S. G., Power C., Robotham A. S. G., 2013, Astronomy and Computing, 3, 23, http://hmf.icrar.org
Navarro J. F., Frenk C. S., White S. D. M., 1996, ApJ, 462, 563
Old L. et al., 2014, MNRAS, 441, 1513
Old L. et al., 2015, MNRAS, 449, 1897
Peng Y.-j. et al., 2010, ApJ, 721, 193
Planck Collaboration et al., 2015, A&A, submitted, arXiv:1502.01589
Robotham A. S. G. et al., 2011, MNRAS, 416, 2640
Rose J. A., 1977, ApJ, 211, 311
Rykoff E. S. et al., 2014, ApJ, 785, 104
Schechter P., 1976, ApJ, 203, 297
Shapley H., 1926, Harvard College Observatory Bulletin, 838, 1
Skibba R. A., van den Bosch F. C., Yang X., More S., Mo H., Fontanot F., 2011, MNRAS, 410, 417
Taylor E. N. et al., 2011, MNRAS, 418, 1587
Tempel E. et al., 2014, A&A, 566, A1
Tinker J., Kravtsov A. V., Klypin A., Abazajian K., Warren M., Yepes G., Gottlöber S., Holz D. E., 2008, ApJ, 688, 709
Tully R. B., Fisher J. R., 1978, in IAU Symposium, Vol. 79, Large Scale Structures in the Universe, Longair M. S., Einasto J., eds., pp. 31–45
Turner E. L., Gott, III J. R., 1976, ApJS, 32, 409
van den Bergh S., 1960, ApJ, 131, 558
van der Marel R. P., 1994, MNRAS, 270, 271
von der Linden A., Wild V., Kauffmann G., White S. D. M., Weinmann S., 2010, MNRAS, 404, 1231
Wang L., Steinhardt P. J., 1998, ApJ, 508, 483
Warren M. S., Abazajian K., Holz D. E., Teodoro L., 2006, ApJ, 646, 881
Weinmann S. M., van den Bosch F. C., Yang X., Mo H. J., 2006, MNRAS, 366, 2
Wilson E. B., 1927, J. of the Am. Stat. Assoc., 22, 209
Wojtak R., Hansen S. H., Hjorth J., 2011, Nature, 477, 567
Wojtak R., Mamon G. A., 2013, MNRAS, 428, 2407
Yang X., Mo H. J., van den Bosch F. C., 2008, ApJ, 676, 248
Yang X., Mo H. J., van den Bosch F. C., 2009, ApJ, 695, 900
Yang X., Mo H. J., van den Bosch F. C., Jing Y. P., 2005, MNRAS, 356, 1293
Yang X., Mo H. J., van den Bosch F. C., Pasquali A., Li C., Barden M., 2007, ApJ, 671, 153
Zwicky F., Herzog E., Wild P., Karpowicz M., Kowal C. T., 1961, Catalogue of galaxies and of clusters of galaxies, Vol. I. California Institute of Tecnhology, Pasadena

Table A1. Coefficients for the approximation of the dilogarithm (eq. [A5])

i	1	2	3	4	5	6	7	8	9	10
a_i	0	1	5	1	131	661	1 327	1 163	148 969	447 047
b_i	1	4	24	6	960	5 760	13 440	13 440	1 935 360	6 451 200

APPENDIX A: RADIAL VELOCITY DISPERSION FOR NFW MODEL WITH ML VELOCITY ANISOTROPY

The expression for the radial velocity dispersion can be obtained from the Jeans equation (14), yielding (van der Marel 1994; Mamon & Łokas 2005)

$$\sigma_r^2(r) = \frac{G}{\nu(r)} \int_r^\infty \exp\left[2\int_r^s \beta(t)\frac{\mathrm{d}t}{t}\right] \nu(s)\frac{M(s)}{s^2}\,\mathrm{d}s\,, \tag{A1}$$

where the term in brackets is expressed in analytical form for simple anisotropy models in an appendix of Mamon et al. (2013).[23] With the anisotropy model of equation (18), the exponential in equation (A1) becomes $(s+r_{200}/c)/(r+r_{200}/c)$. The solution of equation (A1) for a pure NFW model (eq. [16]) with the Mamon & Łokas (2005) velocity anisotropy (eq. [18]) is then

$$\begin{aligned}\frac{\sigma_r^2(r)}{GM_{200}/r_{200}} &= \frac{c/[6\,y\,(y+b)]}{\ln(c+1)-c/(c+1)} \\ &\times \Big\{6\,(3\,b-2)y^2(y+1)^2\mathrm{Li}_2(-y) + 6\,b\,y^4\,\coth^{-1}(2y+1) - 3\,b\,y^2(2y+1)\ln y \\ &\quad +3\,\left[2y\,(y+1)\,(2y+1) - b\,\left(4y^3+8y^2+2y-1\right)\right]\,\ln(y+1) \\ &\quad +(3\,b-2)\,y^2(y+1)^2\left[\pi^2+3\,\ln^2(y+1)\right] + 3\,y\,\left[(4-7b)\,y^2+(5-9\,b)\,y-b\right]\Big\}\,,\end{aligned} \tag{A2}$$

where $y = c\,r/r_{200}$, $b = c\,r_\beta/r_{200}$, while Li_2 is the dilogarithm or Spence function:

$$\mathrm{Li}_2(x) = -\int_0^x \ln(1-u)\,\frac{\mathrm{d}u}{u} = \sum_{i=1}^\infty \frac{x^i}{i^2}\,. \tag{A3}$$

For our choice of $r_\beta = r_{-2}$, i.e. $b=1$, equation (A2) simplifies to

$$\begin{aligned}\frac{\sigma_r^2(r)}{GM_{200}/r_{200}} &= \frac{c/[6\,y\,(y+1)]}{\ln(c+1)-c/(c+1)} \\ &\times \Big\{6\,y^2(y+1)^2\mathrm{Li}_2(-y) + 6\,y^4\,\coth^{-1}(2y+1) - 3\,y^2(2y+1)\ln y + y^2(y+1)^2\left[\pi^2+3\,\ln^2(y+1)\right] \\ &\quad -3\,(2y^2-1)\,\ln(y+1) - 3\,y\,(y+1)\,(3\,y+1)\Big\}\,.\end{aligned} \tag{A4}$$

In equations (A2) and (A4), the dilogarithm of negative argument, $\mathrm{Li}_2(-x)$ can be approximated using series expansions around $x=0$, $x=1$, and $x\to\infty$, yielding

$$\mathrm{Li}_2(-x) \simeq \begin{cases} \displaystyle\sum_{i=1}^{10}(-1)^i\frac{x^i}{i^2} & x < 0.35 \\ \displaystyle -\frac{\pi^2}{12} + \sum_{i=1}^{10}\left(\frac{\ln 2}{i} - \frac{a_i}{b_i}\right)\,(1-x)^i & 0.35 \leqslant x < 1.95 \\ \displaystyle -\frac{\pi^2}{6} - \ln^2(x) + \sum_{i=1}^{10}(-1)^i\frac{x^{-i}}{i^2} & x \geqslant 1.95 \end{cases}\,, \tag{A5}$$

where the coefficients a_i and b_i given in Table A1. Equation (A5) has relative accuracy better than 2.5×10^{-6} for all x. With the approximation of equation (A5) for $\mathrm{Li}_2(-x)$, the radial velocity dispersion σ_r in equation (A4) has relative accuracy better than 10^{-4} for all r.

APPENDIX B: PROJECTED PHASE SPACE DENSITY OF INTERLOPING GALAXIES

We estimate the projected phase space density of interloping galaxies following Mamon et al. (2010), this time using the galaxies from the z=0 output of the SAM of Guo et al. (2011) instead of the dark matter particles of the hydrodynamical cosmological simulation of Borgani et al. (2004).

Figure B1 shows the variations with projected radius of the interloper PPS density parameters A, σ_i and B (defined in eq. [20]). The best fitting parameters are

$$\log_{10} A(X) = -1.092 - 0.01922\,X^3 + 0.1829\,X^6\,, \tag{B1}$$

[23] Even if the halo component is limited to the virial radius r_{200}, the upper integration limit in equation (A1) must be infinity.

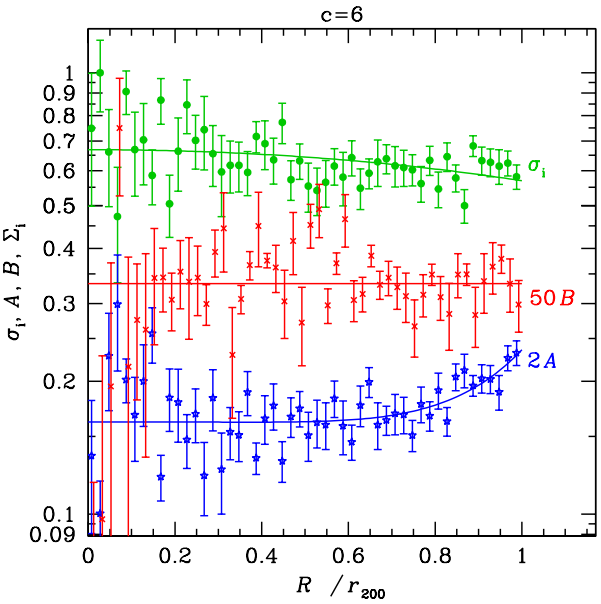

Figure B1. Parameters of the density of interlopers in projected phase space vs. projected radius, taken from the z=0 galaxies of the semi-analytical model of Guo et al. (2011). The values are from maximum likelihood fits, assuming that the scale radius is 1/6th the virial radius, and the error bars represent the uncertainties on these values. the curves are the best fits given by equations (B1), (B2), and (B3).

$$\sigma_{\rm i}(X) = 0.6695 - 0.1004\,X^2\,, \tag{B2}$$

$$B(X) = 0.0067\,, \tag{B3}$$

where $X = R/r_{200}$.

APPENDIX C: SDSS ERRORS ON GALAXY LUMINOSITY AND STELLAR MASS

Despite its very high quality, the SDSS survey is not immune to errors on galaxy stellar mass and luminosity. We estimate these errors below.

C1 SDSS errors on stellar mass

The SDSS-DR10 database contains 8 measures of stellar mass for the primary spectroscopic sample. Figure C1 compares these 8 different measures. Apart from those from the Wisconsin group, the models generally agree to better than 0.3 dex, i.e. the errors on individual masses are of order $0.3/\sqrt{2} = 0.2$ dex. In particular, the MPA/JHU masses agree with all others to typically better than 0.2 dex for σ and 0.3 dex for the rms ($\sqrt{\mu^2+\sigma^2}$). We therefore adopt an error of 0.2 dex on stellar mass.

C2 SDSS errors on galaxy luminosity

Writing the r-band absolute magnitude of a galaxy as

$$M_r = r - \mu(z) - k_r(z) - A_r^{\rm Gal} - A_r^{\rm int} \tag{C1}$$

where μ is the distance modulus, while r, k_r, $A_r^{\rm Gal}$, and $A_r^{\rm int}$ are respectively the apparent magnitude, k-correction, Galactic extinction and internal extinction, all in the r band. The photometric errors are expected to be less than 0.05 mag, i.e. less than 0.02 dex on luminosity. The error caused by the uncertain distance can be written as the quadratic sum of the error on redshift (as a distance indicator) and the neglect of group peculiar velocities relative to the observer. We dot not consider here the galaxy peculiar velocities within a group, as the group finders handle this.

$$\epsilon(\log_{10} L_r) = \frac{1}{\ln 10}\left[\left(\frac{\epsilon(v)}{cz}\right)^2 + \left(\frac{\sigma(v_{\rm p})}{cz}\right)^2\right]^{1/2} \lesssim 0.056\,{\rm dex}$$

for $\epsilon(v) \simeq 30\,{\rm km\,s^{-1}}$, $\sigma(v_{\rm p}) \simeq 200\,{\rm km\,s^{-1}}$, and $z > 0.01$ (where the assumption of zero difference in peculiar velocity between the galaxy and the observer dominates the error). According to Figure 2 of Chilingarian et al. (2010), the intrinsic scatter in the k-correction is of order 0.015 mag, i.e. 0.006 dex. Admittedly, the k-correction of Chilingarian et al. suffers from some catastrophic errors, but since 99.9% of the galaxies with $z < 0.12$ have k-corrections between -0.15 and 0.25, it suffices to impose these limits to k_r. Finally, since SDSS spans

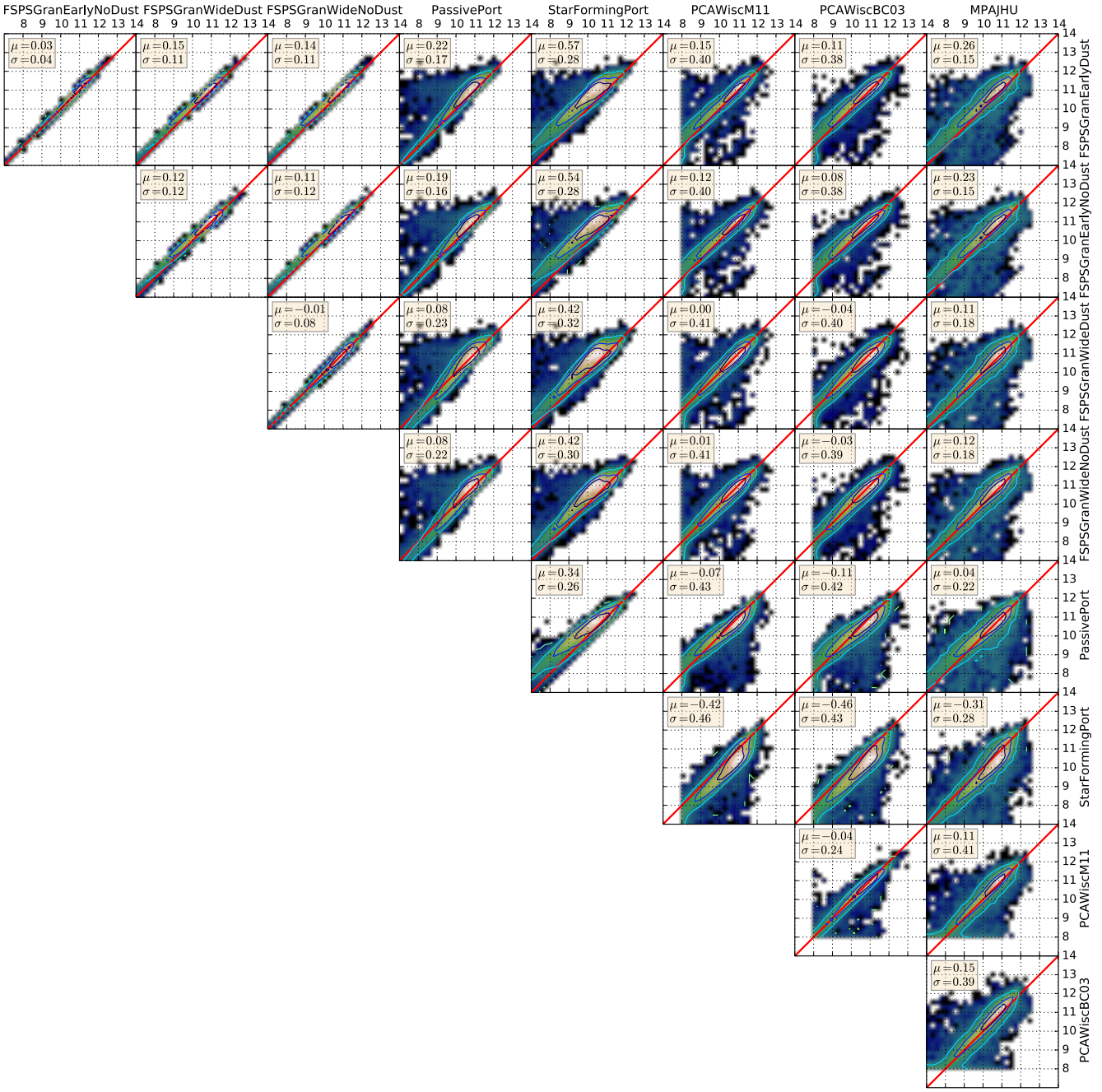

Figure C1. Comparison of the 8 measures of log stellar mass (solar units) in the SDSS-DR10 database. The biases (μ) and bias-corrected differences (σ) are highlighted. These measures are from the following models. FSPSGranEarlyDust, FSPSGranEarlyNoDust, FSPSGranWideDust, and FSPSGranWideNoDust: `logMass` respectively from `stellarMassFSPSGranEarlyDust`, `stellarMassFSPSGranEarlyNoDust`, `stellarMassFSPSGranWideDust`, and `stellarMassFSPSGranWideNoDust` (Conroy et al. 2009); PassivePort and StarFormingPort: `logMass` respectively from `stellarMassPassivePort` and `stellarMassStarFormingPort` (Maraston et al. 2009); PCAWiscM11 and PCAWiscBC03: `mstellar_median` respectively from `stellarMassPCAWiscM11` and `stellarMassPCAWiscBC03` (Chen et al. 2012), respectively using the Maraston & Stromback (2011) and Bruzual & Charlot (2003) stellar population sythesis models; MPAJHU: `lgm_tot_p50` from `GalSpecExtra` (Brinchmann et al. 2004) using the Bruzual & Charlot (2003) stellar population sythesis model.

high galactic latitudes, the uncertainty on the Galactic extinction should be $\simeq 0.075$ mag (the median r-band extinction of SDSS/Legacy galaxies), i.e. 0.03 dex. The uncertainty on internal extinction is more difficult to measure, but can be estimated to be 0.1 mag, i.e. 0.04 dex. Combining these 6 errors (photometry, redshift, assumption of no peculiar velocity, k-correction, Galactic extinction and internal extinction) in quadrature, we deduce that the error on luminosity is of order of 0.08 dex.

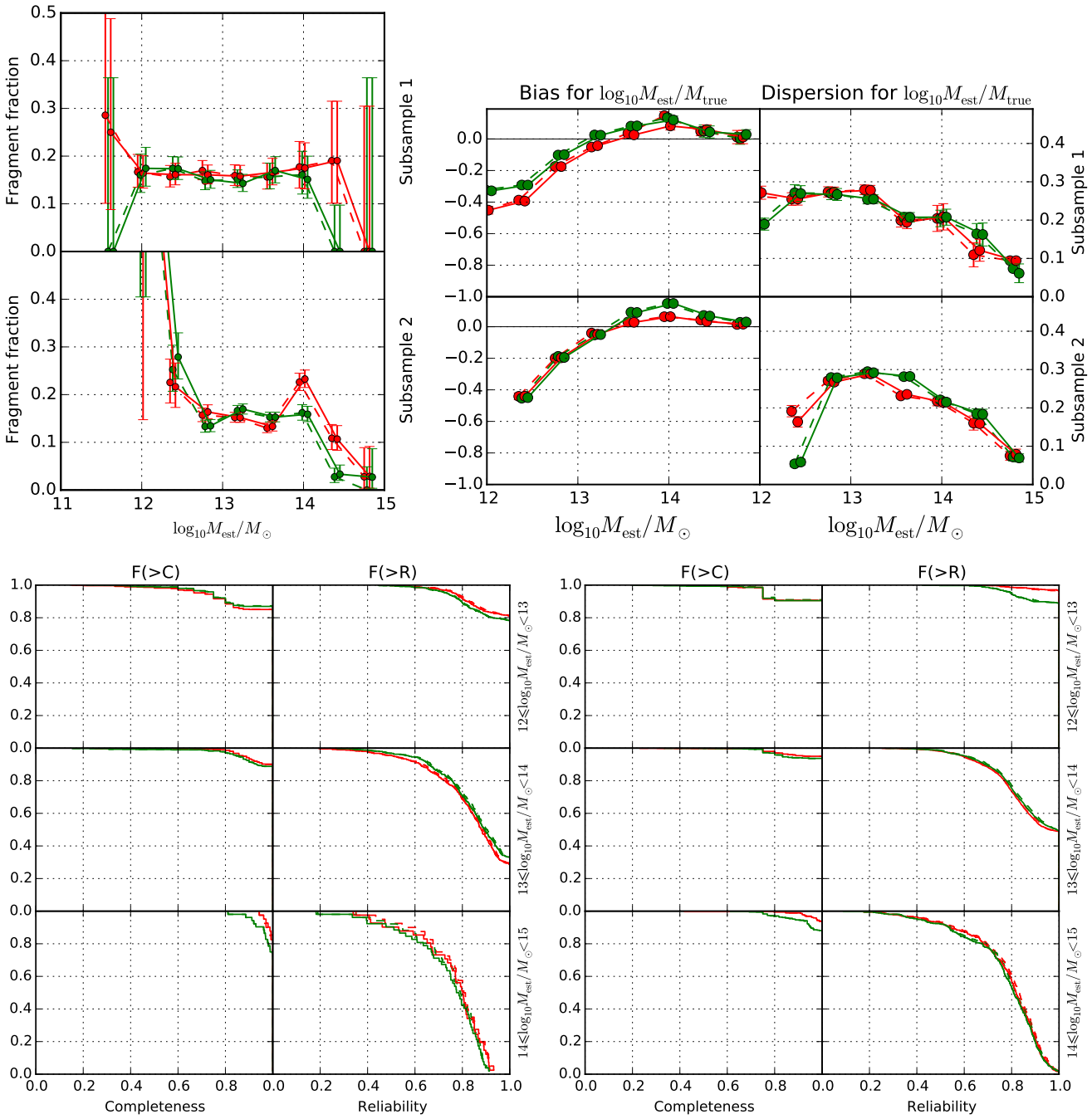

Figure D1. Effects of the choice of the $A(X)$, $\sigma_{\rm i}(X)$ and B entering the expression of the density of interlopers in projected phase space (eq. [20]) on the performance of MAGGIE-L (red) and MAGGIE-M (green), both with observational errors, comparing the expression for $\widehat{g}_{\rm i}(X,u)$ derived by Mamon et al. (2010) on the dark matter particles of a cosmological hydrodynamical simulation (eqs. [21]-[23], *dashed*) with that derived in Appendix B on the galaxies of the semi-analytical of Guo et al. (2011) at $z=0$ (eqs. [24]-[26], *solid*). The analysis is for unflagged groups of at least 3 true and 3 extracted members. The points in the upper plots have their abscissa slightly shifted for clarity.

APPENDIX D: GRAPHICAL REPRESENTATION OF THE EFFECTS OF THE INTERLOPER DENSITY IN PROJECTED PHASE SPACE ON THE PERFORMANCE OF MAGGIE

In this appendix, we illustrate, in Figure D1, the effects of 2 choices for the dimensionless density of interlopers in projected phase space, $\widehat{g}_{\rm i}(X,u)$ (eq. [20]) on the performance of MAGGIE-L and MAGGIE-M. See the discussion in Sect. 5.3.4.

APPENDIX E: DIMENSIONLESS SURFACE DENSITY THRESHOLD FOR THE YANG ET AL. GROUP FINDER

Yang et al. (2005) defined the redshift space local density contrast (relative to the mean density of the Universe) at the edge of the group as

$$\mathcal{B} = \frac{V_{\rm sph}(r_{\rm v})}{V_{\rm cyl}(r_{\rm v})} \frac{\rho(r_{\rm v})}{\rho_{\rm U}} \,, \tag{E1}$$

where the first term represents the ratio of volumes of the virial sphere in real space to the virial cylinder in redshift space, the second term is the local overdensity at the surface of the virial sphere, and the galaxy number density field is assumed to trace the mass density field. With $V_{\rm sph} = 4\pi/3 r_{\rm v}^3$ and $V_{\rm cyl} = 2\,(\sigma_v/H_0)\,\pi r_{\rm v}^2$ (assuming that the cylinder's half-length is σ_v/H_0),[24] and assuming an NFW density profile (eq. [16]), the local mass density at the virial sphere is

$$\rho_{\rm NFW}(r_{\rm v}) = \frac{\Delta\,\rho_{\rm U}}{3\,\Omega_{\rm m}} \frac{[c_\Delta/(c_\Delta+1)]^2}{\ln(c_\Delta+1) - c_\Delta/(c_\Delta+1)} \,, \tag{E2}$$

where Δ is the overdensity of the group relative to the critical density of the Universe, $\rho_{\rm U}$ is the mean density of the Universe, $\Omega_{\rm m}$ is the cosmological density parameter, and c_Δ is the concentration of the group. Combining equations (E1) and (E2), one finds

$$\mathcal{B} = \frac{\sqrt{8\,\Delta}}{9\,\eta\,\Omega_{\rm m}}\, f_{\mathcal{B}}(c_\Delta) \,, \tag{E3}$$

$$f_{\mathcal{B}}(c) = \frac{[c/(c+1)]^2}{\ln(c+1) - c/(c+1)} \,, \tag{E4}$$

where $\eta = \sigma_v/v_{\rm v}$ is the ratio of velocity dispersion to virial velocity for the group.

Yang et al. (2005, 2007) adopted an overdensity of 180 relative to the mean density of the Universe, and use a cosmological N-body simulation with $\Omega_{\rm m} = 0.3$ to calibrate their group finder. This corresponds to an overdensity relative to critical of $\Delta = 0.3 \times 180 = 54$. We can solve for the concentration c_{54} relevant for the median Yang et al. halos, $\log hM_{54,\rm median} \simeq 13.5$ as follows. We loop over values of $\log M_{200}$, for which we extract c_{200} from the relation of Maccio et al. (2008), which also considers h. Assuming the NFW density model, we then solve for c_{54} given c_{200}, as well as M_{54} given M_{200}. Given our derived relation between c_{54} and M_{54}, we solve for the median c_{54}, which yields $c_{54,\rm median} = 8.72$. Then, through equations (E3) and (E4), we obtain $\mathcal{B} = 6.14$, which can be contrasted to $\mathcal{B} = 10$ estimated by Yang et al. (2005) and also adopted by Yang et al. (2007).

We can also apply equations (E3) and (E4) to our case, where $\Delta = 200$, $\Omega_{\rm m} = 0.25$ (the Millennium-II simulation on which the mock catalog was built) and a median halo mass of $\log M_{200,\rm median} \simeq 13.5$ (without the h term). This yields $c_{200,\rm median} = 4.97$ and $\mathcal{B} = 19.9$.

Given that Yang et al. (2005) checked that $\mathcal{B} = 10$ gave them the best results for the groups they extracted from their mock galaxy catalogue (given their groups in real space), we need to rescale their $\mathcal{B} = 10$ to our values of Δ, $\Omega_{\rm m}$ and c. With equations (E3) and (E4), we find $\mathcal{B} = 10 \times [\sqrt{200/54}/(0.25/0.3)] \times [f_B(4.97)/f_B(8.72)] = 29$ (with a factor 2.3 from the first term in brackets and a factor 1.24 from the 2nd term).

We test the effects of the choice of $\mathcal{B}$ in Figure E1. The higher threshold of $\mathcal{B} = 29$ leads to slighter higher group fragmentation (upper left panel), much lower galaxy completeness, but much higher galaxy reliability (lower panels), yet slightly higher dispersion on group total masses (upper right panel).

[24] Equation (E1) with these two formulae for the volumes are analogous to equation (11) of Yang et al. (2005), who seemed to have forgotten the factor 2 for $V_{\rm cyl}$.

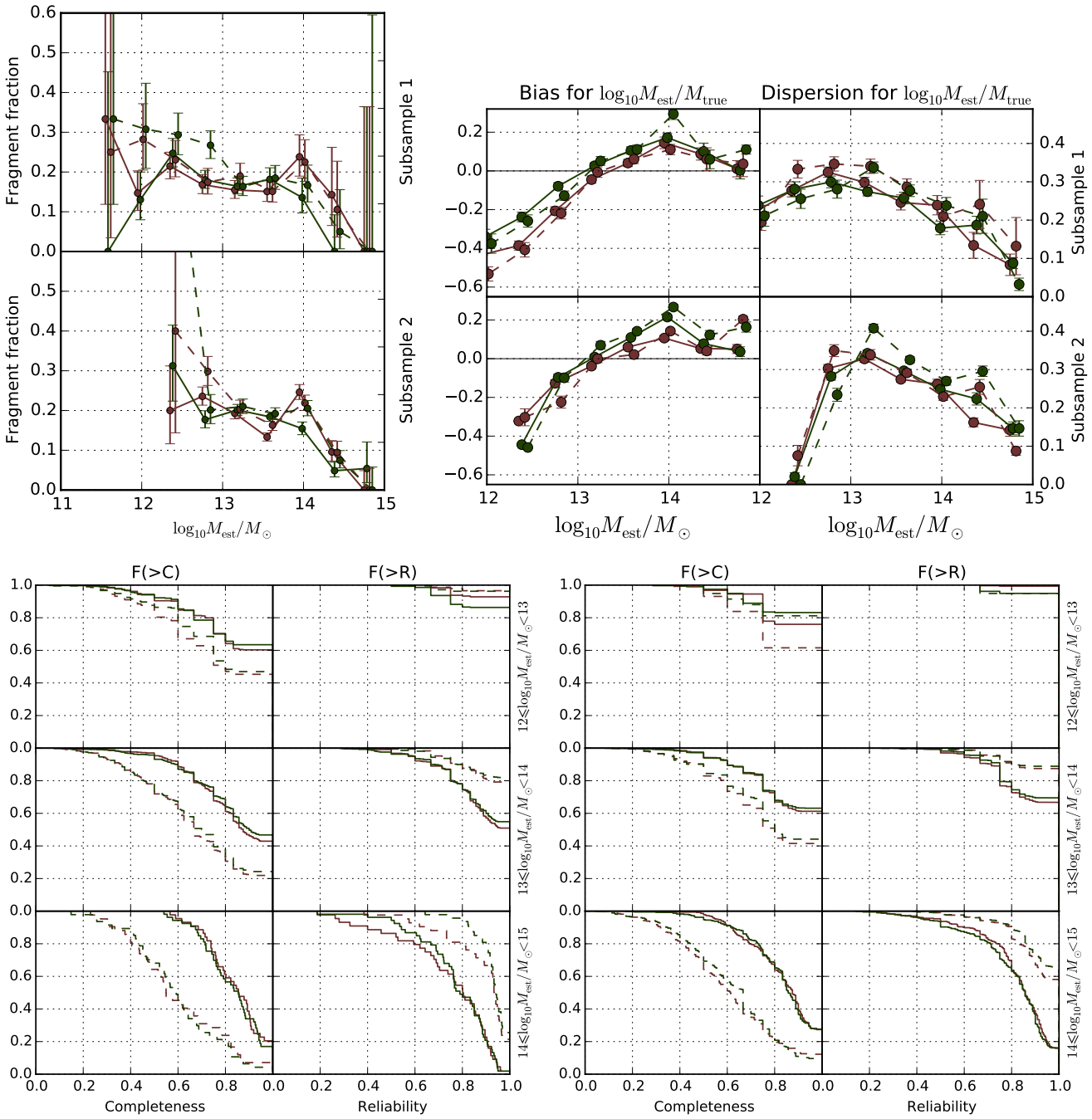

Figure E1. Effects of the choice of the density contrast threshold $\mathcal{B}$ on the performance of our implementation of the Yang et al. group finder, for Yang-L (*brown*), Yang-M (*dark green*), with $\mathcal{B} = 10$ (*solid lines*) and $\mathcal{B} = 29$ (*dashed lines*), both with observational errors. The analysis is for unflagged groups of at least 3 true and 3 extracted members. The points in the upper plots have their abscissa slightly shifted for clarity.